PCCP

First-Principles Calculations of Oxidation Potentials of Electrolytes in Lithium-Sulfur Batteries and Their Variations with Changes in Environment

Journal:	*Physical Chemistry Chemical Physics*
Manuscript ID	CP-ART-05-2018-002912.R1
Article Type:	Paper
Date Submitted by the Author:	23-Jun-2018
Complete List of Authors:	Han, Jaebeom; Texas A&M Engineering, Chemical Engineering Balbuena, Perla; Texas AandM University, Chemical Engineering

First-Principles Calculations of Oxidation Potentials of Electrolytes in Lithium-Sulfur Batteries and Their Variations with Changes in Environment

Jaebeom Han and Perla B. Balbuena*

Department of Chemical Engineering,

Texas A&M University, College Station, TX 77843

* balbuena@tamu.edu

Abstract

Oxidation potentials of electrolyte molecules in Li-Sulfur (Li/S) batteries and their variations in various solvent environments are investigated using first-principles calculations in order to understand oxidative decomposition reactions of electrolytes for cathode passivation. Electrolyte solvents, Li salts, and various additives in Li/S batteries along with some Li-ion battery additives are studied. Oxidation potentials of isolated electrolyte molecules are found to be out of the operating range of typical Li/S batteries. The complexation of electrolyte molecules with Li^+, salt anion, S_8, and pyrene alters oxidation potentials compared to those of the isolated systems. The salt anion lowers oxidation potentials of electrolyte molecules by at least 4.7 % while the complexes with Li^+ have higher oxidation potentials than the isolated molecules by at least 10.4 %. S_8 and pyrene, used as model compounds for sulfur and sulfur/carbon composite cathode materials, also affect oxidation potentials of electrolyte molecules, but their influence is negligible and the oxidation trends differ from those of the Li^+ and salt anion. Although complexations change the oxidation potentials of electrolyte molecules, they are still higher than

the operating voltage range of Li/S batteries, which indicates that oxidation of the studied electrolytes in Li/S batteries is not expected under ambient conditions.

1. Introduction

In order to reduce CO_2 and NOx gases from internal combustion engine (ICE) equipped vehicles, electric vehicles (EVs) are have been developed for transportation, and several commercial electric vehicles from hybrid electric vehicle to full battery electric vehicles are running with the aid of Li-ion batteries. Among these electric vehicles, Model S manufactured by Tesla has the longest driving range of 335 miles with an energy density of 691 Wh/L and the specific energy of 260 Wh/kg.[1] However, they still do not meet the goals for the energy density and the specific energy by the United States Advanced Battery Consortium (USABC) for commercial EVs in 2020, which are 750 Wh/L and 350 Wh/kg for the energy density and the specific energy, respectively.[2] These goals are still challenging with the current insertion electrode materials in Li-ion batteries, and an alternative electrode material with higher capacity is necessary, which is sulfur.[3] Sulfur provides a high theoretical capacity of 1672 mAh g^{-1}, which is much higher than the theoretical capacity of layered transition metal oxide materials (~280 mAh g^{-1}) in Li-ion batteries, and lithium-sulfur (Li/S) batteries also offer a high specific energy of 2500 Wh kg^{-1}.[3]

In spite of this high capacity, there are obstacles for commercial uses of Li/S batteries. First is the shuttle mechanism of intermediate redox species of sulfur, lithium polysulfides (PS hereafter), which are dissolved into electrolyte, diffuse to the anode, and have chemical reactions on the anode surface.[3-4] In addition, the dissolution of PS into electrolyte causes a self-discharge while in the resting state, leading to a capacity fading.[4] These problems originate from the

dissolution of PS into the electrolyte from the cathode. In order to resolve the PS dissolution, two routes can be utilized; the electrode (cathode) design and the electrolyte design. Of these two routes, the electrolyte design is so far the most explored, and especially additives are investigated which may be able to form a protective layer on the cathode surface through oxidative decomposition.

Several research groups have investigated the cathode passivation electrolyte additives in Li-ion batteries in order to prevent electrolyte decomposition on the cathode surface[5-25] and to improve the thermal stability of cathodes.[26-27] In Li/S batteries, however, there are only a few studies on developing electrolyte additives to protect the cathode surfaces and to prevent the dissolution of PS into the electrolyte and the resultant the polysulfide shuttle reaction. Kim and co-workers reported the use of alph-lipoic acid (ALA)[28] and 3,4-ethylenedioxythiophene (EDOT)[29] to prevent the chemical reaction between the polysulfide and the Li metal anode by formation of polymer films covering the cathode surface. Shao and co-workers also showed that the polymerization of pyrrole to polypyrrole forms a protective layer for the cathode and suppresses the polysulfide diffusion.[30] Yushin and co-workers employed the lithium iodide (LiI) additive to form a protective layer on both cathode and anode surfaces to hinder the direct contact with electrolyte solvent and to suppress the polysulfide dissolution.[31] They also generated a Li-ion conducting protective layer by the electrochemical reduction of fluoroethylene carbonate (FEC), and the layer served as a polysulfide barrier to suppress the polysulfide migration from the cathode into the electrolyte.[32]

In this study, we investigate oxidation potential variations of electrolyte molecules with various environments in Li/S batteries as an initial step toward the understanding of oxidative decompositions of electrolyte molecules. The considered molecules are electrolyte solvents,

including 1,2-dimethoxyethane (DME) and 1,3-dioxolane (DOL), Li salt anions, including bis(fluorosulfonyl)imide anion (FSI^-) and bis(trifluoromethanesulfonyl)imide anion ($TFSI^-$), and four additives (EDOT, FEC, I^-, and pyrrole) studied for cathode passivation layer formation in Li/S batteries mentioned above. Two distinct conformations of DME are considered in this study; one has a staggered conformation for two methoxide groups along the C-C bond (DME_ttt hereafter), and the other has a gauche conformation for two methoxide groups (DME_tgt hereafter). In addition, the two most widely studied additives (BOB^- and $DFOB^-$) in Li-ion batteries are also considered in this study in order to test if they could be applied for Li/S batteries. The molecular structures considered in this study are displayed in Figure 1 except I^-. This manuscript starts with the details of density functional theory (DFT) calculations in Section 2. In Section 3, we compare oxidation potentials of electrolyte molecules both in the isolated case and in complexes with Li cation (Li^+) and Li salt anion ($TFSI^-$) together with in complexes with S_8 and pyrene, which are model compounds for S/C cathode materials used in Li/S batteries. Then, Section 4 wraps up with summary and conclusions.

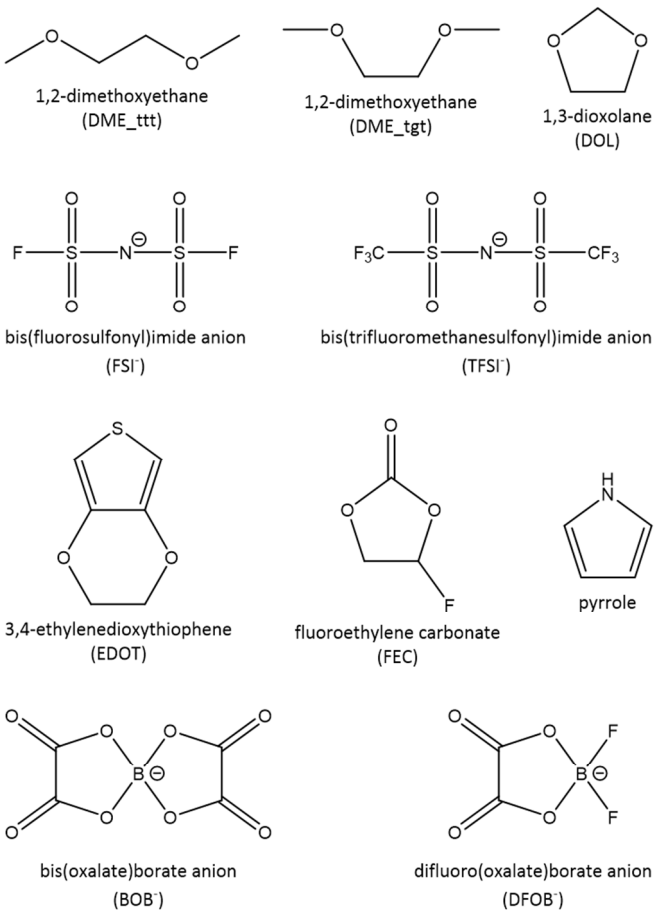

Figure 1. Structures of electrolyte molecules investigated for oxidation potentials in this study.

2. Computational Details

Geometry optimizations and frequency calculations are performed using a DFT method. Of various DFT methods, three hybrid functional methods, including B3PW91,[33-34] BMK,[35] and M06-2X,[36] are selected for a benchmark test of redox potential calculations. The 6-311G(d,p) basis set[37] and its various polarization and diffusion combinations up to 6-311++G(3df, 3pd), Dunning's correlation consistent triple zeta basis set, cc-pVTZ[38] and its augmented basis set, aug-cc-pVTZ,[39] and Truhlar's calendar basis sets, including may-, jun-, and jul-cc-pVTZ,[40] are also considered for the benchmark calculation. The BMK/cc-pVTZ theoretical level yields the lowest mean unsigned error (MUE) compared to experimental redox potentials in the benchmark

calculation, and this method is employed in this study. Because the cc-pVTZ basis set does not apply to iodine, other basis sets and effective core potentials (ECPs) were also tested for geometrical parameters of I_2 and I_2^- molecules, ionization potential and electron affinity of iodine, and oxidation potential of iodide, and the LanL2DZdp ECP[41-42] was chosen for iodine.

In order to consider the solvent effect, the SMD solvation model[43] is employed with tetrahydrofuran (THF) for solvent because THF is the ether solvent with the dielectric constant (ε= 7.43) close to those of DME and DOL, which are 7.30 and 7.34, respectively. Frequency calculations are carried out in order to check the stationary points of optimized geometries. The Gibbs free energy is obtained at 298 K. All computations are carried out using the Gaussian 09 program.[44] For complexes, the various sets of initial geometries are generated using the Absorption Locator module in Materials Studio.[45] The empirical dispersion correction can be considered for more accurate oxidation calculations of complex systems using Grimme's DFT-D3 methods, implemented in Gaussian 09 as GD3[46] and GD3BJ[47]; however, the correction by including dispersion interaction was found to be less than 1.0 % in our test calculations. Therefore, no empirical dispersion correction for complex systems was added in this study.

The oxidation potentials are calculated based on the thermodynamic cycle shown in Scheme 1. Then, the oxidation potential is calculated using Eq. (1), and is subtracted from 1.37 in order to convert the absolute potential scale to the Li/Li^+ scale.[48]

$$E_{\mathrm{ox}}^{0}(\text{vs. } \mathrm{Li/Li^+}) = \Delta G_{\mathrm{ox}}^{0}/F - 1.37 = [\Delta G_{\mathrm{e}} + \Delta G_{\mathrm{sol}}^{0}(\mathrm{A^+}) - \Delta G_{\mathrm{sol}}^{0}(\mathrm{A})]/F - 1.37 \qquad (1)$$

where ΔG_{e} is the free energy of ionization in the gas phase, $\Delta G^0_{\mathrm{sol}}(\mathrm{A})$ is the solvation free energy of species A, $\Delta G^0_{\mathrm{sol}}(\mathrm{A}^+)$ is the solvation free energy of the oxidized A (A^+), and *F* is the Faraday constant.

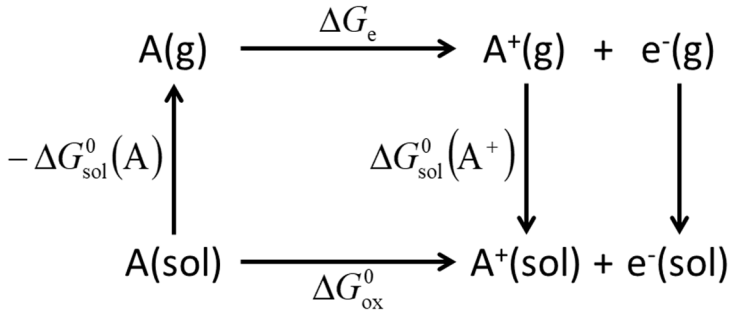

Scheme 1. Thermodynamic cycle for the oxidation reaction, where (g) denotes the gas phase, and (sol) denotes the solution phase.

3. Results

The calculated oxidation potentials are listed in Table 1. Not only oxidation potentials of isolated electrolyte solvents, anions, and additives but also those of complexes with Li^+, Li salt anion, Li salt, S_8, and pyrene are also listed.

Table 1. Oxidation potentials of isolated electrolyte solvents, anions, and additives together with those of complexes with Li^+, $TFSI^-$, LiTFSI, S8, and pyrene, calculated at the BMK/cc-pVTZ theoretical methods with the SMD solvation model

	Oxidation Potential (V)						
	Calculation						Experiment
	Isolated	Complexed					
		w/ Li^+	w/ $TFSI^-$	w/ LiTFSI	w/ S_8	w/ Pyrene	
DME_ttt	5.26	6.14 (+0.88)	4.60 (-0.66)	5.27 (+0.01)	5.34 (+0.08)	4.11 (-1.15)	4.6[49], 5.1[50]
DME_tgt	5.16	6.71 (+1.55)	4.74 (-0.42)	5.84 (+0.68)	5.22 (+0.06)	4.33 (-0.83)	
DOL	5.74	6.74 (+1.00)	4.53 (-1.21)	5.79 (+0.05)	5.65 (-0.09)	4.26 (-1.48)	5.2[50]
FSI^-	5.81	7.04 (+1.23)	--	--	5.36 (-0.45)	3.91 (-1.90)	> 4.5[51]
$TFSI^-$	5.68	6.99 (+1.31)	--	--	5.41 (-0.27)	4.01 (-1.67)	5.3[52]

EDOT	4.62	5.23 (+0.61)	4.26 (-0.36)	4.93 (+0.31)	--	--	3.95[29]
FEC	7.47	8.60 (+1.13)	5.72 (-1.75)	6.89 (-0.58)	--	--	5.0[53]
I^-	3.42	4.31 (+0.89)	--	3.86 (+0.44)	3.39 (-0.03)	3.20 (-0.22)	3.0[31]
Pyrrole	4.43	5.34 (+0.91)	3.95 (-0.48)	4.93 (+0.50)	4.37 (-0.06)	4.11 (-0.32)	0.92[54] (vs. $Ag/AgNO_3$)
BOB^-	5.79	6.39 (+0.60)	--	6.09 (+0.30)	--	--	4.5[55]
$DFOB^-$	5.44	6.58 (+1.14)	--	6.17 (+0.73)	--	--	4.35[56]

3.1. Oxidation Potentials of Isolated Molecules

Compared to the operating voltage range of Li/S batteries, 1.5 V-3.0 V, oxidation potentials of isolated electrolyte molecules are much higher. (Table 1) The optimized geometries both in the initial state and in the oxidized state in the solution phase are displayed in Figure 2 with atoms having significantly positive spin density values highlighted in magenta, which are obtained from the Hirshfeld population analysis.[57] The atomic partial charges are also listed in Table S1 from the CM5 method[58] together with spin density values.

Ross and co-workers reported 4.11 V for the oxidation potential of DME in a common supporting electrolyte with ε=78 using the B3LYP/6-31+G(d) theoretical level with the PCM solvation model.[59] Borodin and co-workers calculated oxidation potentials of DME to 5.66 V and 5.70 V for two conformations of DME, tgt and ttt, respectively, in acetone (ε=20) using the G4MP2 method and the SMD solvation model.[48] Comparing the dielectric constant value in this study with those of Ross and co-workers and Borodin et al., the current calculated oxidation potential of DME is reasonable. The oxidized DME has lengthened bond distances between two methylene C atoms (C6-C9 in Figure 2a and C1-C4 in Figure 2b) from 1.52 Å and 1.52 Å for DME_ttt and DME_tgt, respectively, to 1.75 Å and 1.71 Å for DME_ttt and DME_tgt, respectively, as reported by Ross and co-workers[59] and Borodin and co-workers.[48] The distances of the two C-O bonds (C5-O6 and C9-O12 in Figure 2a, and C1-O8 and C4-O7 in Figure 2b) decrease from 1.40 Å to 1.32 Å for DME_ttt and 1.33 Å for DME_tgt while Ross and co-workers reported that one of them lengthened and the other one shortened.[59] O atoms and the middle C atoms (O5, C6, C9, and O12 in Figure 2a, and C1, C4, O7, and O8 in Figure 2b) have positive spin densities in the oxidized state, and O atoms have higher spin densities than C atoms, which indicates that the O radical is more favorable than the C radical. (Table S1)

DOL has an oxidation potential of 5.74 V, higher than that of DME, as Ross and co-workers reported before.[59] The C3 atom has shorter bond distances with the adjacent O10 and O11 atoms by oxidation from 1.39 Å and 1.40 Å to 1.33 Å, and two C atoms (C1 and C2) get closer from 1.55 Å to 1.53 Å. The distances between O atoms and methylene C atoms increase from 1.41 Å and 1.42 Å to 1.45 Å. (C1 and O10, and C2 and O11) In addition, the H8 and H9 atoms attached to the C3 atom are loosened from 1.09 Å and 1.10 Å to 1.13 Å. The largest positive spin density values are located on O10 and O11 atoms, which means that the electron on the O atom is removed by oxidation. (Figure 2 and Table S1)

Two isolated Li salt anions are predicted to have oxidation potentials of 5.81 V (FSI^-) and 5.68 V ($TFSI^-$). Borodin and co-workers predicted the oxidation potential of FSI^- to be 5.97 V and 6.31 V using the G4MP2 method and the LC-ωPBE/6-31+G(d,p) method, respectively,[48] which is higher than that in this study. In addition, they also predicted higher oxidation potential for $TFSI^-$ to 5.71 V and 6.02 V using the G4MP2 method and the LC-ωPBE/6-31+G(d,p) method, respectively,[48] compared to the one in this study. By oxidation, FSI^- and $TFSI^-$ break their C_2 symmetry along the axis through the N atom in the initial states. (Figures 2d and 2e) In addition, the distances between N and two S atoms in FSI^- and in $TFSI^-$ increase from 1.57 Å (N1-S2 and N1-S3 in FSI^-) and 1.58 Å (N1-S2 and N1-S3 in $TFSI^-$) to 1.65 Å (FSI^-), and 1.65 Å and 1.66 Å ($TFSI^-$). Meanwhile, the distances between S and O atoms are slightly reduced from 1.43 Å (FSI^-) and 1.44 Å ($TFSI^-$) to 1.41 Å (S3-O4 and S3-O5 in FSI^-) and 1.42 Å (S2-O6 and S2-O7 in FSI^-), and 1.42 Å (S3-O5 in $TFSI^-$) and 1.43 Å (S2-O6, S2-O7, and S3-O4 in $TFSI^-$). The distances between S and F atoms in FSI^- decrease by oxidation from 1.59 Å to 1.54 Å (S2-F8) and 1.55 Å (S3-F9). The distances between S and C atoms in $TFSI^-$, however, they are slightly lengthened from 1.87 Å to 1.88 Å (S2-C9) and 1.89 Å (S3-C8) due to oxidation, while the distances of six

C-F bonds are negligibly decreased from 1.32 Å and 1.33 Å to 1.31 Å, which indicates that further oxidations may generate decomposed CF_3 group from $TFSI^-$. The N atoms both in FSI^- and in $TFSI^-$ have positive spin densities, which indicate that unpaired electrons are located on the N atoms. (Figures 2d-e and Table S1)

For additives in Li/S batteries, there is no dramatic bond distance change by oxidation as in DME. (Figures 2f-h) The computed oxidation potential of EDOT is 4.62 V, higher than the experimental oxidation potential of 3.95 V in the 1.0M LiTFSI DME/DOL electrolyte with the SUS electrode.[29] The geometric parameter changes are asymmetric in EDOT by oxidation. The bond distances between S5 and two adjacent C atoms (C1 and C4) change from 1.74 Å to 1.68 Å (C1-S5) and 1.78 Å (C4-S5). The distance between C atoms in the thiophene ring on the one side changes from 1.36 Å to 1.42 Å (C1-C2) while that on the other side slightly decreases from 1.36 Å to 1.35 Å (C3-C4). The C-C bond (C2-C3) increases slightly from 1.44 Å to 1.46 Å. In addition, the C-O bonds on the one side of dioxane ring change from 1.34 Å to 1.28 Å (C2-O9), and from 1.42 Å to 1.46 Å (C13-O9) while those on the other side change from 1.35 Å to 1.33 Å (C3-O8), and from 1.42 Å to 1.43 Å (C10-O8). The C10-C13 bond distance in dioxane ring and all of the bonds related to H atoms (C1-H6, C4-H7, C10-H11, C10-H12, C13-H14, and C14-H15) are found to have negligible changes by oxidation. Positive spin densities are located on atoms highlighted in Figure 2f, and spin density values on four atoms are similar with each other although the C1 atom has the highest spin density.

FEC is predicted to have an oxidation potential of 7.47 V. Lian and co-workers reported that the FEC-containing electrolyte shows no extinct oxidation peak up to 5.1 V in the 1M $LIPF_6$ EC/DMC/DEC (1:1:1 in volume) electrolyte.[10] Considering a dielectric constant value as in THF and comparing to those of EC, DMC, and DEC solvents in the experiment, the high oxidation

potential calculated in this study looks reasonable. The bond distance between C1 atom and F9 atom decreases from 1.37 Å to 1.32 Å while the bond distances between O atoms and alkyl C atoms increase by oxidation from 1.39 Å (C1-O6) and 1.43 Å (C2-O5) to 1.48 Å and 1.48 Å, respectively. The C7-O8 bond in the carbonyl group increases from 1.19 Å to 1.28 Å by oxidation while distances between carbonyl C7 atom and two O atoms (O5 and O6) decrease from 1.33 Å (atoms 5 and 7) and 1.35 Å (atoms 6 and 7) to 1.26 Å and 1.27 Å. The bond length between C1 and F9 decreases from 1.37 Å to 1.32 Å by oxidation, which means that F^- or F• cannot be generated by further oxidations. The carbonyl O8 atom has a positive spin density, which indicates that the electron is removed from the carbonyl O8 atomic site by oxidation.

Iodide has an oxidation potential of 3.42 V in this study while Yushin and co-workers reported value measured in both 5M LiTFSI DME and 5M LiTFSI DOL electrolyte, and calculated oxidation potentials at Møller-Plesset 2nd-order perturbation theory (MP2) and coupled cluster singles doubles perturbative triples (CCSD(T)) method with SDD basis set of iodide are around 3.0 V.[31] However, oxidation potentials obtained using DFT functionals, including B3LYP, M05-2X, and M06-L, with the SDD basis set are 3.77 V, 3.80 V, and 3.71 V, respectively, which are higher than this study.

The calculated oxidation potential of pyrrole is 4.43 V in this study. The oxidation potential of pyrrole monomer was measured to 0.92 V vs. $Ag/AgNO_3$ in 0.1M $AgNO_3$ acetonitrile (35.95 for dielectric constant) electrolyte.[54] Considering that the potential for $Ag/AgNO_3$ reference electrode is 0.337 V vs. saturated calomel electrode (SCE) as stated in Ref 29 and that of SCE vs. the standard hydrogen electrode (SHE) is 0.24 V,[60] the oxidation potential of pyrrole is re-calculated to 1.50 V vs. standard hydrogen electrode (SHE). Then, the converted oxidation potential of pyrrole vs. Li/Li^+ from the experiment is 4.55 V using the Li/Li^+ potential

of -3.05 V vs. SHE, which is higher than the calculated oxidation potential in THF solvent. The bond distances between two adjacent C atoms (C2-C5 and C3-C7) are lengthened from 1.38 Å to 1.43 Å while N-C bond (N1-C2 and N1-C3) distances and C5-C7 bond distance are shortened from 1.36 Å and 1.43 Å to 1.35 Å and 1.37 Å, respectively. Positive spin densities are located on C2 and C3 atoms by oxidation as shown in Figure 2h and Table S1, which is consistent with the polymerization mechanism.[61]

The calculation predicts the oxidation potential of the isolated BOB anion to be 5.79 V, which is lower than that from Wachtler and co-workers, 5.98 V, using the B3LYP/6-311++G(d,p) theoretical method with the conductor polarizable continuum model (C-PCM) with the dielectric constant of 60.0 for the solvation effect.[62] The optimized geometry of BOB^- shows a bond breakage in one of oxalate groups by oxidation from 1.55 Å to 1.85 Å. (C1 and C2, Figure 2i) This bond breakage is also reported from other computational researches by Wachtler and co-workers and Xing and co-workers.[63] With the increase in distance between C1 and C2 atoms in the oxidized oxalate group, the distances between the B5 atom and two O atoms (O8 and O9) in the oxidized oxalate group also increase from 1.46 Å to 1.51 Å. Meanwhile, the distances between C atoms and O atoms decrease from 1.31 Å to 1.25 Å (C1-O9 and C2-O8), and from 1.19 Å to 1.16 Å (C1 and O11 and C2 and O10). This indicates that further oxidation of BOB^- leads to carbon dioxide (CO_2) evolution.[64] The geometric parameters of the other oxalate group of BOB^- in the oxidized state remain almost unchanged, compared to those in the initial state. C and O atoms (C1, C2, O10, and O11) have positive spin density, and the largest spin densities are located on the outer O atoms (O10 and O11), which indicates that the O atoms are the most susceptible to oxidation.

The isolated $DFOB^-$ shows to have an oxidation potential of 5.44 V, which is lower than those by Borodin and co-workers, obtained at G4MP2 (5.72 V) and LC-ωPEB/6-31+G(d,p) (6.10 V) theoretical methods.[48] Just as in the isolated $BOB\ molecule^-$, the C1-C2 bond distance and B-O bond distances increase from 1.56 Å to 1.87 Å (C1-C2), and from 1.49 Å to 1.54 Å (O5-B9 and O6-B9). Also, the distances of two types of C-O bonds decrease from 1.31 Å to 1.25 Å (C1-O5 and C2-O6), and from 1.20 Å to 1.17 Å (C1-O3 and C2-O4). This also indicates that $DFOB^-$ generates CO_2 gas by oxidation.[65-66] B-F bond distances decrease from 1.38 Å to 1.34 Å (F7-B9 and F8-B9) by oxidation. The positive spin densities are located on the oxalate C and O atoms (C1, C2, O3, and O4), and O atoms have the highest spin density values just as in BOB^-. (Figure 2j and Table S1)

	Initial State	Oxidized State
(a)	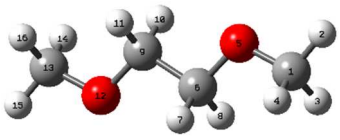	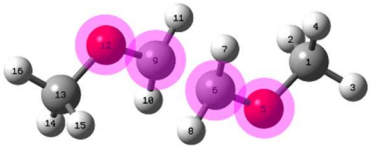
(b)	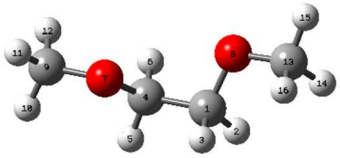	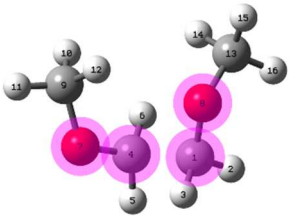
(c)	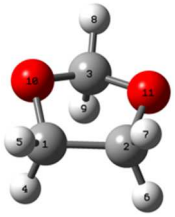	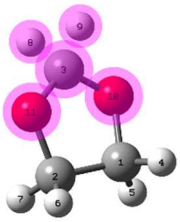

(d)	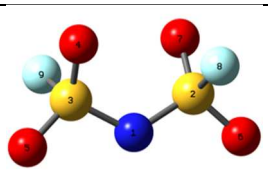	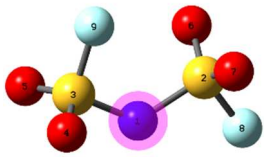
(e)	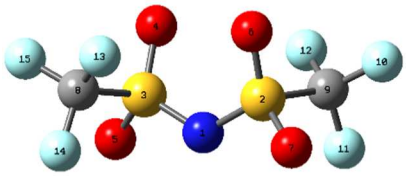	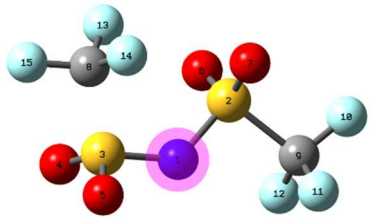
(f)	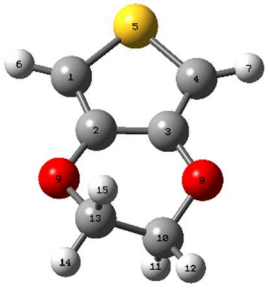	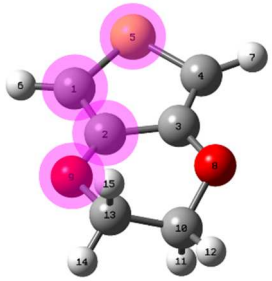
(g)	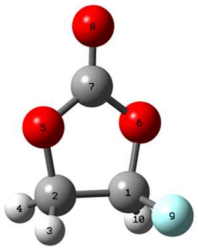	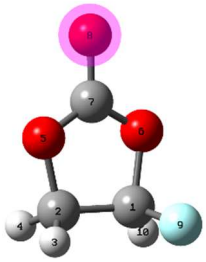
(h)	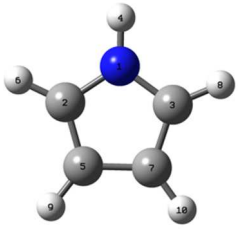	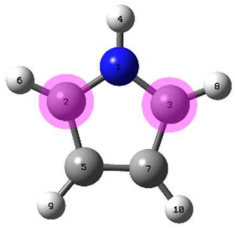
(i)	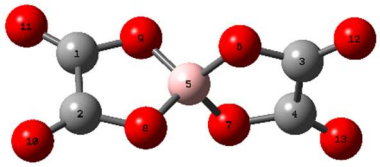	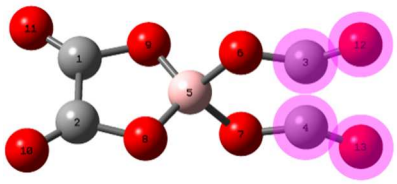

(j)	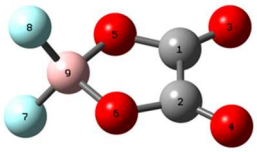	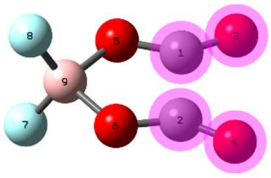

Figure 2. Optimized Geometries of Isolated Solvents, Anions, and Additives both in the Initial and Oxidized States in the Solution Phase. White, peach, grey, blue, red, cyan, and yellow colors represent H, B, C, N, O, F, and S atoms, respectively. The atoms with significant positive spin densities by oxidation are highlighted in magenta.

3.2. Oxidation Potentials of Complexes with the Li cation (Li^+)

Optimized geometries of complexes with Li^+ are listed in Figure 3. The atoms with positive spin density by oxidation are also highlighted, and electrons on electrolyte molecules are removed by oxidation. CM5 charges and spin density values are listed in Table S2. Oxidation potentials of Li^+ complexes are enhanced by 13.2 % through 30.0% from those of isolated systems. This indicates that Li^+ improves the oxidative stabilities of the electrolyte molecules, and this is because of the instability of oxidized molecules caused by repulsion interactions between positive charges on oxidized molecules and on Li^+. By oxidation, charges of neutral electrolyte molecules, including DME_ttt, DME_tgt, DOL, EDOT, FEC, and pyrrole, range from 1.05e to 1.15e, and Li^+'s in DME_ttt/Li^+, DME_tgt/Li^+, DOL/Li^+, EDOT/Li^+, FEC/Li^+. Meanwhile, pyrrole/Li^+ complexes have charges between 0.85e and 0.95 e, both of which are quite close to +1.00e, and lead to repulsive electrostatic interactions between oxidized electrolyte molecules and Li^+. For Li salts, including LiFSI, LiTFSI, LiI, LiBOB, and LiDFOB, although the oxidized anions have much smaller positive charges (between 0.11e and 0.24e) than the above mentioned neutral molecules, oxidation breaks the neutrality between the negative charges

on anions and positive charge on Li^+, resulting in raising oxidation potentials from those of the isolated anions.

The oxidation potential of DME_ttt/Li^+ and DME_tgt/Li^+ complexes are calculated to be 6.14 V and 6.71 V, respectively, which are enhanced compared to those of the isolated DME_ttt and DME_tgt by 16.7 % and 30.0 %, respectively. The DME_ttt/Li^+ complex shows a different conformation for DME_ttt compared to that of the isolated DME_ttt due to oxidation. Meanwhile, the oxidized DME_tgt/Li^+ complex has a similar geometry for DME_tgt compared to the isolated DME_tgt. (Figures 2a-b and 3a-b) Positive spin densities are located on four atoms as in the isolated DME_ttt and DME_tgt, but they are not symmetric around the lengthened C-C bond because of the location of Li^+. (Figures 3a-b and Table S2) The distance between Li17 and O5 atom increases from 1.84 Å to 2.00 Å in the DME_ttt/Li^+ complex, and the distances between the Li17 and O7 atoms in DME_tgt/Li^+ complex increase from 1.88 Å to 1.99 Å in DME_tgt. The main difference between DME_ttt/Li^+ and DME_tgt/Li^+ is the bidentate chelation of Li^+ in the DME_tgt/Li^+ complex in the initial state. This difference is also shown in the locations of the highest occupied molecular orbitals (HOMOs) in Figures S1 and S2, where the HOMO of DME_ttt/Li^+ is almost localized on a site where Li^+ is not located while the HOMO of DME_tgt/Li^+ is completely delocalized over DME_tgt. Although the bidentate chelated Li^+ is the most stable conformation for the DME_tgt/Li^+ complex in the initial state, the oxidized complex has a mono-dentate chelation as shown in Figure 3b. The C-C bonds increase from 1.52 Å and 1.52 Å to 1.73 Å (C6-C9) and 1.69 Å (C1-C4) for the DME_ttt/Li^+ and DME_tgt/Li^+ complexes, respectively. These distances are shorter than those in isolated DME_ttt and DME_tgt. O atoms not chelated with Li^+ have the largest positive spin densities of

0.34 (O12 in Figure 3a) and 0.36 (O8 in Figure 3b) for DME_ttt/Li^+ and DME_tgt/Li^+, respectively.

The DOL/Li^+ complex has an oxidation potential of 6.74 V, higher than that of the isolated DOL by 17.4 %. DOL is oxidized in the complex from locations of positive spin densities in the oxidized state, and this is consistent with the location of the HOMO, delocalized over DOL in the DOL/Li^+ complex. (Figure 3c, Table S2, and Figure S3) The distance between Li12 and O10 atom increases from 1.84 Å to 2.02 Å by oxidation. The C-O bond distances (C3-O10 and C3-O11) decrease from 1.44 Å and 1.37 Å to 1.37 Å and 1.35 Å, and the C1-C2 bond distance also decreases from 1.54 Å to 1.53 Å. The C-H bonds (C3-H8 and C3-H9) have increased bond distances from 1.09 Å and 1.10 Å to 1.11 Å and 1.13 Å while other C-H bonds (C1-H4, C1-H5, C2-H6, and C2-H7) have negligible distance changes. Just as in DME_ttt/Li^+ and DME_tgt/Li^+ complexes, the Li^+-coordinated O10 atom has a smaller spin density than the free O11 atom.

The oxidation potentials of the LiFSI and LiTFSI salts are 7.04 V and 6.99 V, respectively, which are higher than those of isolated FSI^- and $TFSI^-$ by 21.2 % and 23.1 %, respectively. The anions are mainly oxidized in the complexes, and positive spin densities are located on N atoms in the anions, which is also consistent with the HOMO locations found for the LiFSI and LiTFSI salts. (Figures 3d-e, Table S2, and Figures S3-S4) LiFSI and LiTFSI yield different geometries for the oxidized states; LiTFSI retains the bi-dentate coordination in the oxidized state while LiFSI loses one coordination between Li10 and O7 atom by oxidation (Figures 3d-e). The distance between the Li10 and O4 atoms in LiFSI increases from 1.87 Å to 1.95 Å, and the distances between the Li17 and O atoms (O4 and O6) increase from 1.86 Å and 1.87 Å to 2.01 Å and 2.00 Å by oxidation. Although the S-F bonds (S2-F8 and S3-F9) in LiFSI

are shortened from 1.57 Å to 1.53 Å by oxidation, the S-C bonds (S2-C9 and S3-F8) in LiTFSI are lengthened from 1.87 Å to 1.90 Å, which is also observed in the isolated $TFSI^-$. Both salts have positive spin densities located on N atoms as shown in Figures 3d-e.

The EDOT/Li^+ complex also has a higher oxidation potential than the isolated EDOT from 4.62 V to 5.23 V with EDOT oxidized. Positive spin densities are located on the same positions as in the isolated EDOT, and the HOMO is also located only on EDOT. (Figure 3f, Table S2, and Figure S6) Two C-S bonds have asymmetric changes in distance from 1.74 Å to 1.68 Å (C1-S5), and from 1.74 Å to 1.78 Å (atoms 1 and 4 in Figure 3f). Also, two C-C bonds in the thiophene ring also show asymmetric bond distance changes from 1.36 Å to 1.42 Å (atoms 1 and 2), and from 1.36 Å to 1.34 Å by oxidation, as in the isolated EDOT. Distance changes in C-O bonds in dioxane ring are also asymmetric, and the bond lengths change from 1.35 Å to 1.28 Å (atoms 2 and 9), from 1.37 Å to 1.35 Å (atoms 3 and 8), from 1.44 Å to 1.45 Å (atoms 8 and 10), and 1.42 Å to 1.46 Å (atoms 9 and 13). The distance between the Li^+ and the O atom (atom 8) increases from 1.89 Å to 1.96 Å. Positive spin densities are located on four atoms as highlighted in Figure 3f, and the C atom next to S atom (atom 1) has the highest spin density among them.

The oxidation potential of FEC/Li^+ complex is predicted to be 8.60 V, higher by 15.1 % than that of the isolated FEC. FEC is also mainly oxidized from the locations of positive spin densities and HOMO. (Table S2 and Figure S7) Unlike the isolated FEC, where the carbonyl O atom has the highest spin density, positive spin densities are located on four atoms, including C2, H3, H4, and O5. (Figure 3g) Oxidation notably alters the location of Li^+, and the angle between Li^+ and C7 changes from 147.0° to 178.6°. The carbonyl C-O bond length decreases from 1.21 Å to 1.17 Å, and one of two C-O bonds (C7-O6) also has a decreased length from 1.33 Å to 1.29 Å by oxidation while the bond length of the other C-O bond (C7-O5) increases from 1.30 Å to 1.44

Å. This bond length change suggests the decomposition of FEC and the release of CO_2 by oxidation. This claim can be verified from the bond length changes between C1 and O6, and between C2 and O5, where the latter decreases from 1.44 Å to 1.32 Å, and the former increases from 1.41 Å to 1.43 Å. Just as in the isolated FEC, the bond length between C1 and F9 also decreases from 1.35 Å to 1.33 Å by oxidation.

LiI has an enhanced oxidation potential of 4.31 V, compared to that of I^- by 26.0 %, and also shows a lengthened distance between Li^+ and I^- due to oxidation from 2.57 Å to 2.84 Å. (Figure 3h) I^- is oxidized to I• as expected from the location of HOMO, and a positive spin density is located on I•. (Figure S8 and Table S2)

The oxidation potential also increases for pyrrole to 5.34 V by complexation. For the pyrrole/Li^+ complex, Li^+ is stabilized by π-electrons on the aromatic pyrrole ring. By oxidation, however, one of the six π-electrons is removed, and the oxidized pyrrole is not aromatic any more from the Hückel's [4*n*+2] rule. (6 π-electrons → 5 π-electrons) Just as in the isolated pyrrole, positive spin densities are located on the C2 and C3 atoms adjacent to the N1 atom, which indicates that one of π-electrons on C=C bonds (C2-C5 and C3-C7) is removed by oxidation. (Figure 3i and Table S2) This is also confirmed by the increased distances two C=C bonds from 1.38 Å to 1.44 Å while the bond lengths of N1-C2 and N1-C3 decrease from 1.37 Å and 1.36 Å to 1.34 Å and 1.35 Å, respectively. The distance between the center of mass of pyrrole and Li^+ increases from 1.91 Å to 4.23 Å by oxidation. (Figure 3i)

The oxidation potentials of LiBOB and LiDFOB are 6.39 V and 6.58 V, increased by 10.4 % and 21.0 % compared to those of isolated BOB^- and $DFOB^-$, respectively. From the locations of HOMOs in LiBOB and LiDFOB in Figures S10 and S11, BOB^- and $DFOB^-$ are oxidized in these complexes, and this is verified from the locations of positive spin densities in

Figures 3j-k. LiBOB retains the bidentate chelation of Li^+ to the oxalate group by oxidation while the chelation by O atoms in the oxalate group is broken, and Li^+ has an interaction with the F atom in LiDFOB. (Figures 3j-k) The bond length between C1 and C2 in the unchelated oxalate group increases from 1.55 Å to 1.85 Å in LiBOB, and that of C-C bond in the oxalate group in LiDFOB also increases from 1.54 Å to 1.87 Å. All C-O bond lengths in the unchelated oxalate group in LiBOB decrease from 1.32 Å to 1.26 Å (C1-O9), from 1.19 Å to 1.16 Å (C1-O11), from 1.32 Å to 1.26 Å (C2-O8), and from 1.19 Å to 1.16 Å (C2-O10) while the B-O bond lengths increase from 1.44 Å to 1.49 Å (B5-O8 and B5-O9). In LiDFOB, all C-O bonds in the oxalate group also have decreased bond lengths by oxidation as in LiBOB, but B-O bond lengths also slightly decrease from 1.52 Å to 1.51 Å on the contrary to those in LiBOB. F-B bond lengths change asymmetrically by Li^+ to 1.33 Å (F7-B9) and 1.38 Å (F8-B9) from 1.36 Å. Distances between Li^+ and the O atoms in LiBOB increase from 1.99 Å to 2.07 Å (Li^+-O12) and 2.06 Å (Li^+-O13).

	Initial State	Oxidized State
(a)	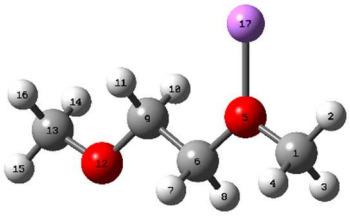	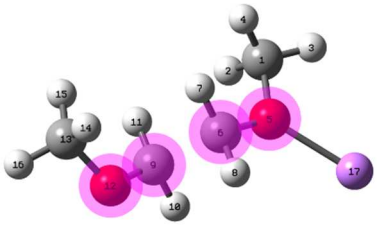
(b)	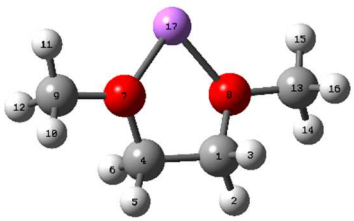	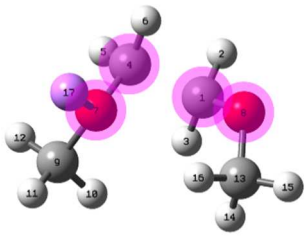

(c)	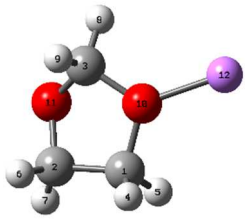	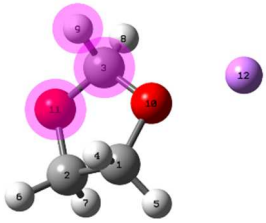
(d)	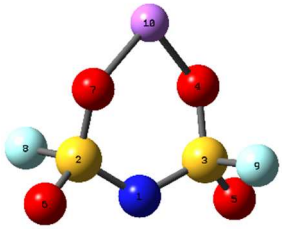	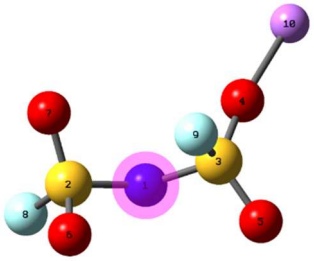
(e)	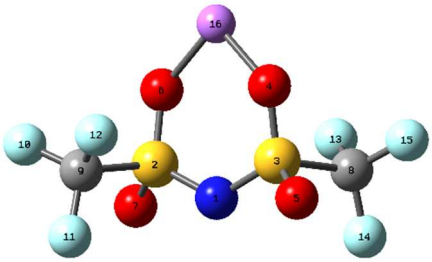	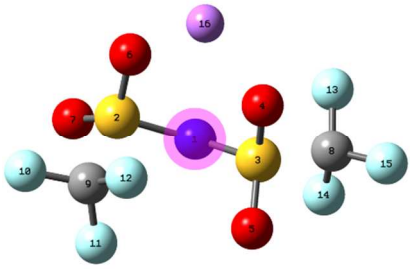
(f)	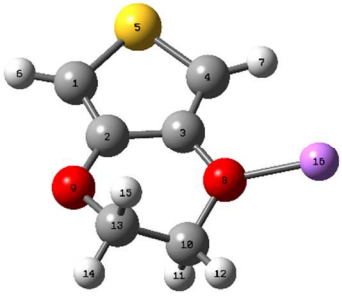	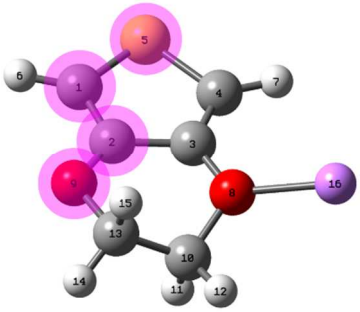

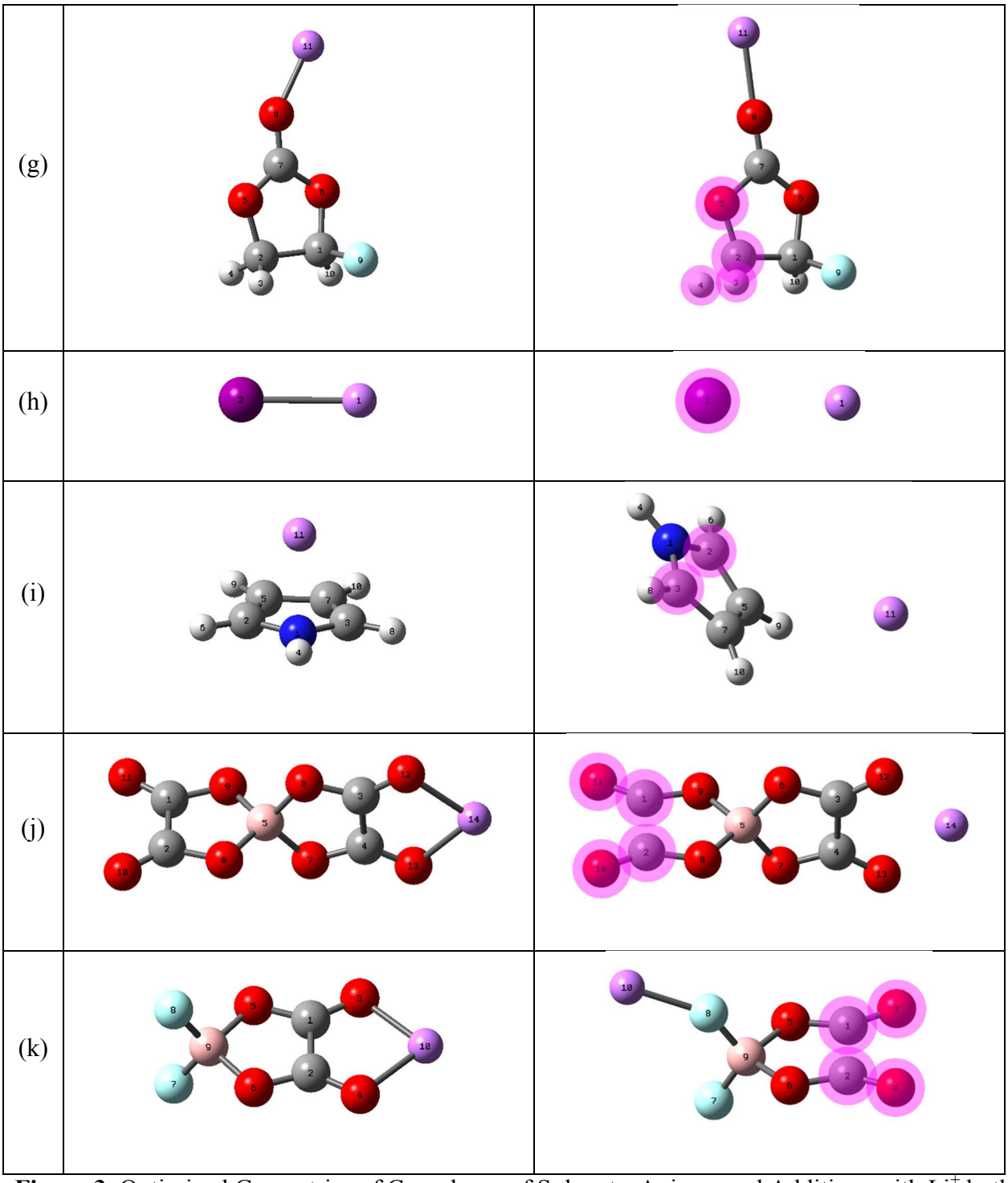

Figure 3. Optimized Geometries of Complexes of Solvents, Anions, and Additives with Li^+ both in the Initial and Oxidized States in the Solution Phase. (White, violet, peach, grey, blue, red, cyan, and yellow colors represent H, Li, B, C, N, O, F, and S atoms, respectively, and the atoms with significant positive spin densities by oxidation are highlighted in magenta.)

3.3. Oxidation Potentials of Complexes with Li Salt Anion ($TFSI^-$)

There have been various studies showing that oxidation potentials of electrolyte molecules are lowered with the explicit existence of anions.[48, 67-70] In our calculations, oxidation potentials of neutral electrolyte molecules, including DME_ttt, DME_tgt, DOL, EDOT, FEC, and pyrrole, are also reduced by the complexation with $TFSI^-$ by 7.8 % through 23.4 % compared to those of isolated cases. Li salts complexed with $TFSI^-$, including LiI/$TFSI^-$, LiBOB/$TFSI^-$, and LiDFOB/$TFSI^-$, also have reduced oxidation potentials, compared to those of Li salts by 4.7 % through 10.4 %. These reductions originate from the stabilization of positive charges on oxidized species by negative charge on $TFSI^-$. (Table S3) Although oxidation potentials of electrolyte molecules are lowered when complexed with an anion, these reductions still are not enough to lay the oxidation potentials of molecules investigated in this study within the operating voltage of Li/S batteries. However, adding more anions can help lower oxidation potentials and place then within the operating voltage.[70]

Oxidation potentials for DME_ttt/$TFSI^-$, DME_tgt/$TFSI^-$, and DOL/$TFSI^-$ complexes are calculated to be 4.60 V, 4.74 V, 4.53 V, respectively. (Table 1) They are reduced compared to those of the isolated DME_ttt, DME_tgt, and DOL by 12.5 %, 8.1 %, and 21.1 %, respectively. HOMOs are located on electrolyte solvent molecules as shown in Figures S1-S3, and positive spin densities are also located in solvent molecules (Figures 4a-c and Table S3); therefore, solvent molecules are mainly oxidized in these complexes. Oxidized states show H-transferred geometries from solvent molecules to the anion as highlighted by the red dotted circle in Figures 4a-c. The zero-point energy corrected potential energy differences of the H-transferred geometries from the non-H-transferred geometries are -4.7 kcal/mol, -1.4 kcal/mol, and -18.6

kcal/mol for DME_ttt/$TFSI^-$, DME_tgt/$TFSI^-$, and DOL/$TFSI^-$ complexes, respectively, which indicates that the H transfer produces the most stable geometries by oxidation in solvent/$TFSI^-$ complexes. Calculations for complexes with FSI^- are not shown here because they have the same trends and similar values for oxidation potentials. However, the H transfer is also observed in solvents/FSI^- complexes. Oxidized DME_ttt, DME_tgt, and DOL have 0.11e, 0.09e, and 0.14e for charges, respectively, and the $TFSI^-$ has charges of -0.11e, -0.09e, and -0.14e. Charges of both solvents and salt anion are very close to zero, not close to +1 for solvents and -1 for anion, which indicates that proton (H^+) is transferred from the oxidized positively charged solvent molecules to the negatively charged $TFSI^-$, and the protonated $TFSI^-$ (TFSIH) is generated. This is also verified by the fact that highest spin densities are located on H-detached C atoms in DME_ttt, DME_tgt, and DOL. (Table S3) In addition, the interaction energy and free energy change for the formation of TFSIH ($TFSI^- + H^+ \rightarrow$ TFSIH) are calculated to be -144.1 kcal/mol and -138.5 kcal/mol at BMK/cc-pVTZ, which means that the protonation of $TFSI^-$ in solution is very favorable and spontaneous. These huge values of the interaction energy and free energy change favor the oxidation of solvent molecules when complexed with $TFSI^-$.

Although the proton transfer is favored in the solvent/$TFSI^-$ complexes, no proton-transferred geometry is observed in the neutral additive complexes with $TFSI^-$. Among these neutral additives, FEC shows an opposite trend to EDOT and pyrrole. EDOT and pyrrole are mainly oxidized as suggested by the charge changes and the spin density values as in the solvent molecules while $TFSI^-$ is mainly oxidized with FEC. (Table S3 and Figures 4d-f) From the HOMO energy level comparison, FEC has the lowest HOMO energy in the electrolyte molecules in this study (-0.37 Hartree), which means that FEC is the most stable against oxidation, and the HOMO electron of $TFSI^-$ is more susceptible to oxidation in the FEC/$TFSI^-$ complex. However,

the HOMO energies of both EDOT (-0.25 hartree) and pyrrole (-0.25 hartree) are higher than that of $TFSI^-$ (-0.31 hartree); therefore, EDOT and pyrrole are oxidized when complexed with $TFSI^-$. Oxidation potentials of EDOT and pyrrole are reduced by about 7.8% and 10.8% when complexed with $TFSI^-$, becoming 4.26 V and 3.95 V, respectively. However, the oxidation potential of FEC/$TFSI^-$ complex is calculated to be 5.72 V, which is increased by 0.7 % from that of the isolated $TFSI^-$. This discrepancy arises from the fact that the oxidized FEC/$TFSI^-$ complex has no stabilization effect by electrostatic interaction between the neutral FEC and the neutral oxidized $TFSI^-$ while the oxidized EDOT and pyrrole are stabilized by the negative charge on $TFSI^-$. CM5 charges of oxidized EDOT and pyrrole are 0.85e and 0.83e, close to +1.00e, and those of $TFSI^-$ are -0.84e and -0.83e, close to -1.00e, in EDOT/$TFSI^-$ and pyrrole/$TFSI^-$ complexes, respectively, while the oxidized FEC/$TFSI^-$ complex has CM5 charges of 0.11e and -0.11e, both of which are close to 0.00e, leading to much weaker electrostatic stabilization.

	Initial State	Oxidized State
(a)	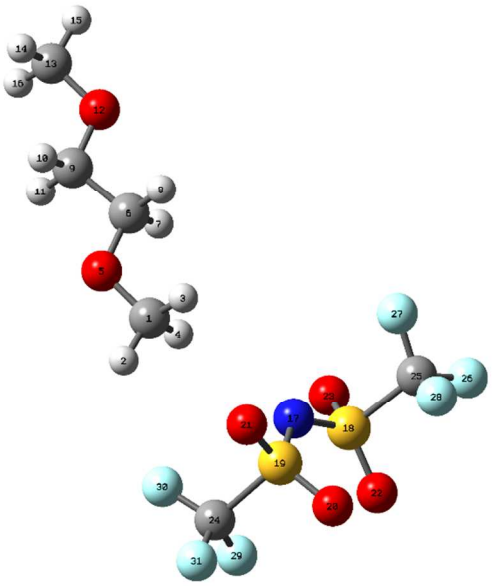	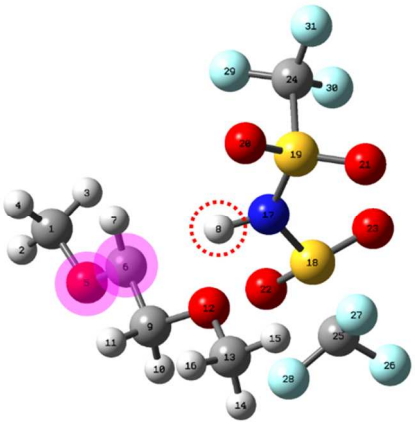

(b)	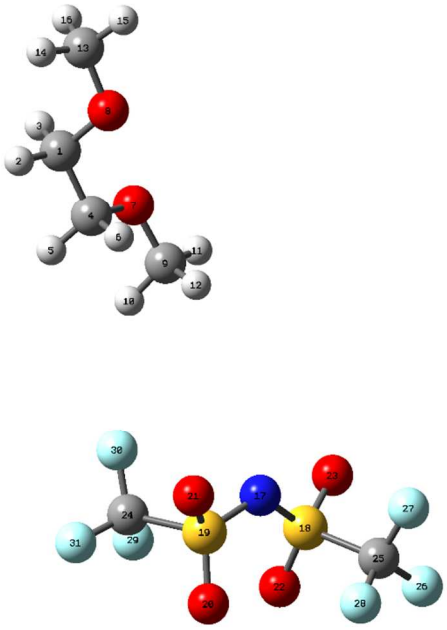	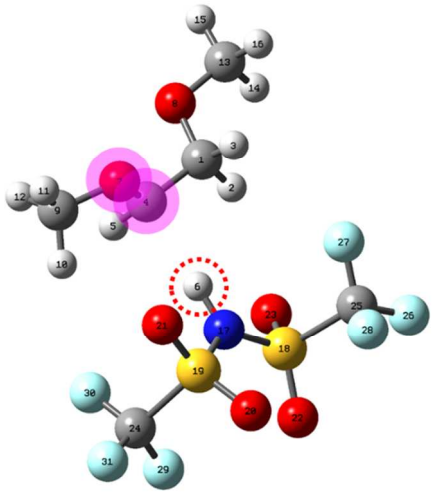
(c)	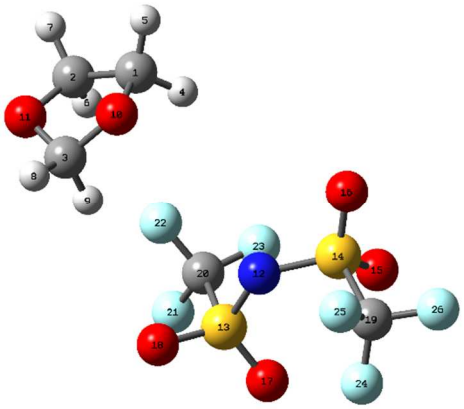	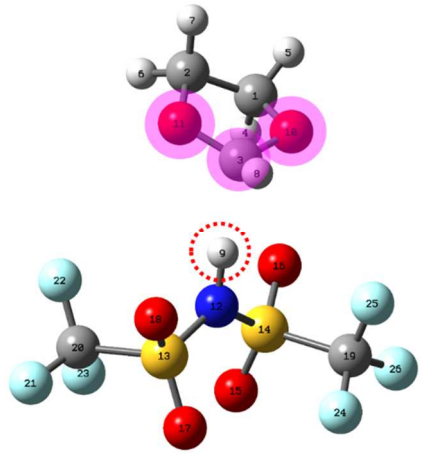

(d)	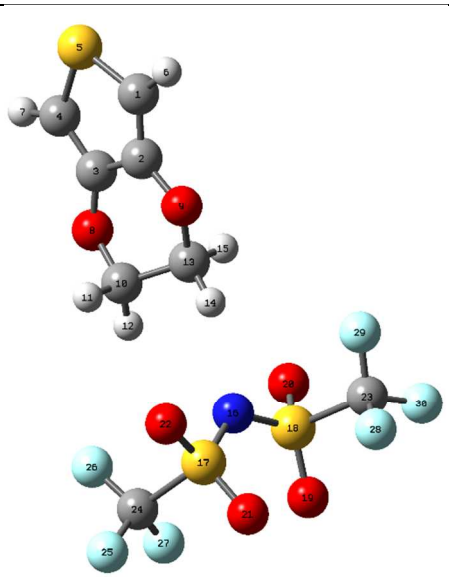	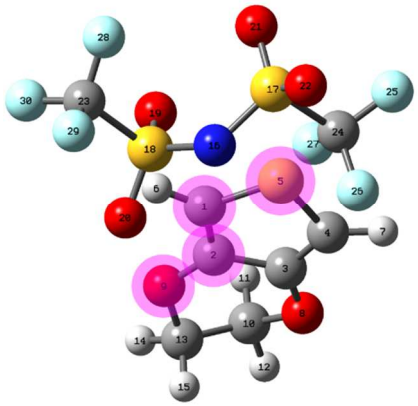
(e)	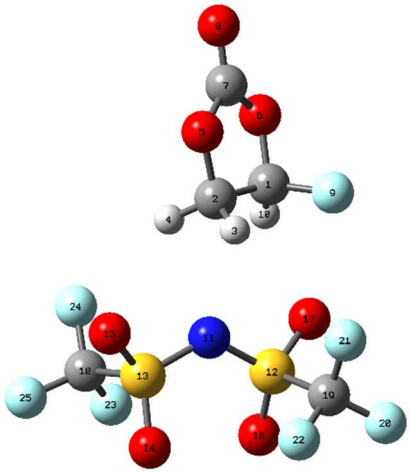	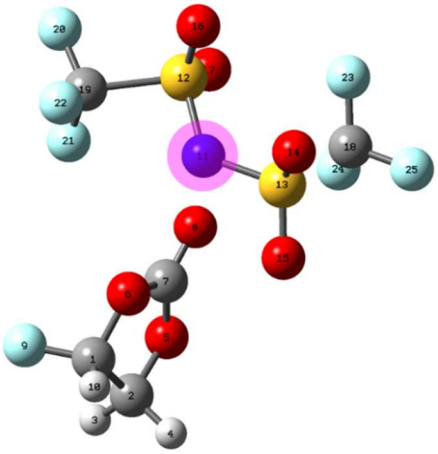

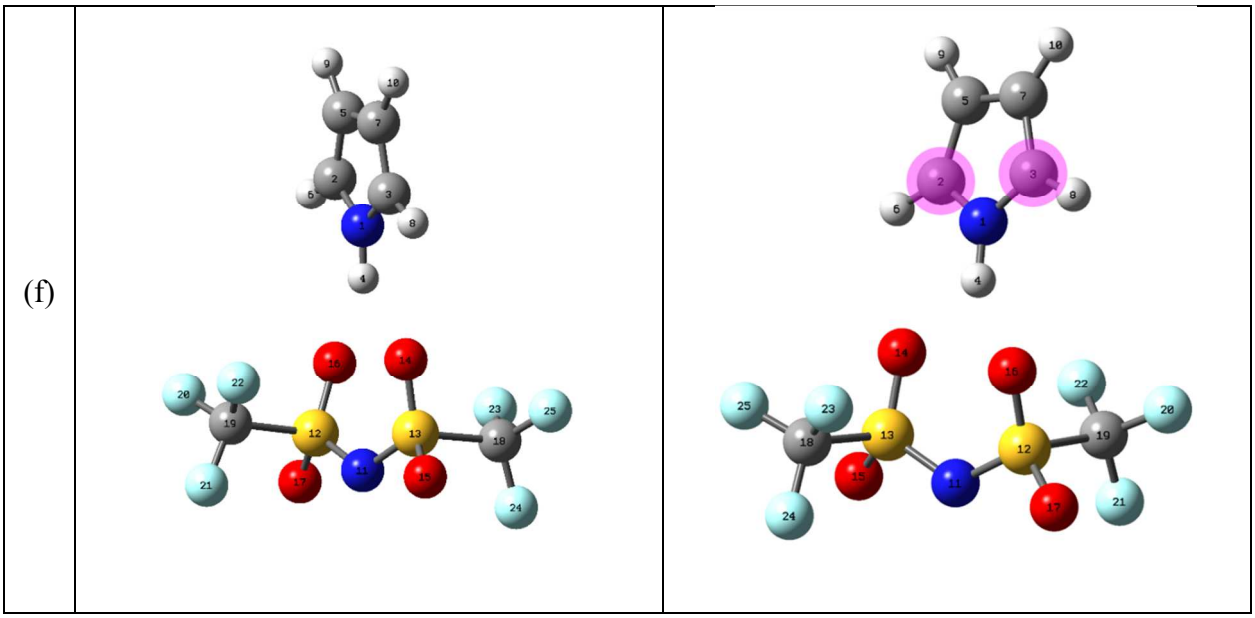

Figure 4. Optimized Geometries of Complexes of Solvents and Additives with $TFSI^-$ both in the Initial and Oxidized States in the Solution Phase. (White, violet, grey, blue, red, cyan, and yellow colors represent H, Li, C, N, O, F, and S atoms, respectively. The atoms with significant positive spin densities by oxidation are highlighted in magenta, and H atoms circled in red are transferred to $TFSI^-$.)

3.4. Oxidation Potentials of Complexes with Li Salt (LiTFSI)

In previous sections, the effects of Li^+ and $TFSI^-$ on the oxidation potentials of the electrolyte molecules are described separately. However, the contact ion-pair between Li^+ and $TFSI^-$ can also observed in the electrolyte solution[71]; therefore, the oxidation potentials of electrolyte complexes with LiTFSI are considered in this section.

The solvent/LiTFSI complexes have oxidation potentials of 5.27 V, 5.84 V, and 5.79 V, for DME_ttt/LiTFSI, DME_tgt/LiTFSI, and DOL/LiTFSI, respectively, which lie between the oxidation potentials of the solvent/$TFSI^-$ complexes and those of the solvent/Li^+ complexes. However, deviations from oxidation potentials of isolated solvent molecules are not very large as

shown in Table 1. Solvent molecules are oxidized in complexes as in the complexes with Li^+ and $TFSI^-$ (Figures 5a-c and Table S4). Locations of HOMOs are also localized on solvent molecules as in solvent/$TFSI^-$ complexes (Figures S1-S3). It is also observed that the proton transfer is favorable as shown in Figures 5a-c as in the solvent/$TFSI^-$ complexes in the previous section. This proton transfer facilitates the delocalization of the positive charge on the oxidized solvent molecules to the whole complexes. Comparing the partial charges of solvents, Li^+, and $TFSI^-$, not only solvent molecules but also $TFSI^-$ have a positive partial charge by the proton transfer in the oxidized state from -0.32e, -0.36e, and -0.33e to 0.16e, 0.17e, and 0.20e for DME_ttt/LiTFSI, DME_tgt/LiTFSI, and DOL/LiTFSI, respectively.

Just as in the previous section, the FEC/LiTFSI complex also has the opposite oxidation trend to EDOT/LiTFSI and pyrrole/LiTFSI complexes as shown in Figures 5d-f and Table S4. Oxidations of EDOT and pyrrole are predicted at 4.93 V and 4.93 V in the complexes, respectively; however, $TFSI^-$ is also oxidized in the FEC/LiTFSI complex at 6.89 V. Just as in the complexes with $TFSI^-$, HOMOs are located on EDOT and pyrrole in the EDOT/LiTFSI and pyrrole/LITFSI complexes while the FEC/LiTFSI complex has a HOMO located on $TFSI^-$ (Figures S6-S7, and S9) EDOT/LiTFSI and pyrrole/LiTFSI complexes also have lower oxidation potentials than complexes with Li^+, and higher oxidation potentials than complexes with $TFSI^-$. The CM5 partial charges in the oxidized state for the EDOT/LiTFSI are 1.10e, 0.20e, and -0.30e for EDOT, Li^+, and $TFSI^-$, respectively, and those for pyrrole/LiTFSI complexes are 1.05e, 0.25e, and -0.30e for pyrrole, Li^+, and $TFSI^-$, respectively. This indicates that the repulsions between the oxidized additives and Li^+ are mitigated by the opposite negative charge on $TFSI^-$ and oxidation potentials are lowered than those for complexes with Li^+. The location of Li^+, however, enlarges the repulsion between Li^+ and the oxidized $TFSI^-$ in the FEC/LiTFSI complex, and the

oxidation potential is enhanced compared to that for the FEC/TFSI$^-$ complex. CM5 partial charges for the oxidized FEC/LiTFSI complex are 0.13e, 0.36e, and 0.51e for FEC, Li^+, and TFSI$^-$, respectively.

Oxidation potentials of I$^-$/LiTFSI, BOB$^-$/LiTFSI, and DFOB$^-$/LiTFSI complexes are 3.86 V, 6.09 V, and 6.17 V, which also lie between the oxidation potentials for isolated anionic additives and Li-salt forms. From the locations of the HOMOs and the positive spin densities, I$^-$, BOB$^-$, and DFOB$^-$ are also oxidized in these complexes. (Figures 5f, h-i, Figures S8, S10-S11, and Table S4) CM5 partial charges for the I-/LiTFSI complex in the oxidized state are 0.21e, 0.54e, and -0.75e. The BOB$^-$/LiTFSI complex in the oxidized state has CM5 partial charges of 0.20e, 0.13e, and -0.33e, and the DFOB$^-$/LiTFSI complex has 0.04e, 0.65e, and -0.69e for partial charges in the oxidized state. Then, the negative charges on TFSI$^-$ stabilize the positive charges on oxidized anionic additives and Li^+, leading to the decrease in the oxidation potential, compared to LiI, LiBOB, and LiDFOB.

	Initial State	Oxidized State
(a)	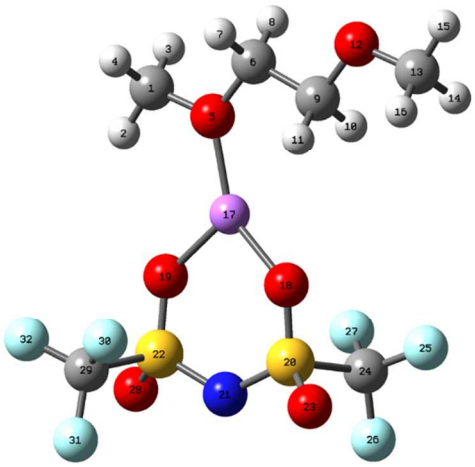	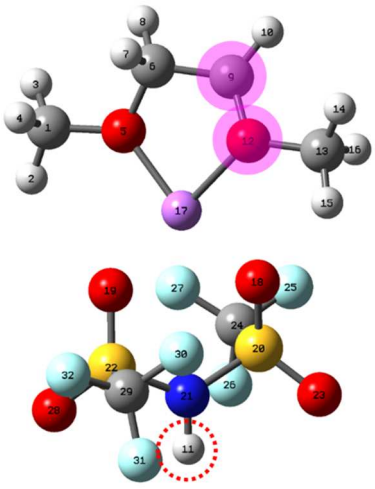

(b)	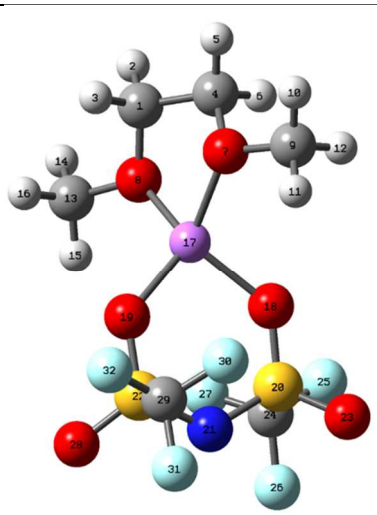	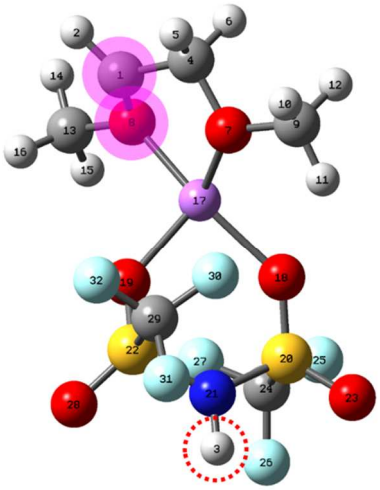
(c)	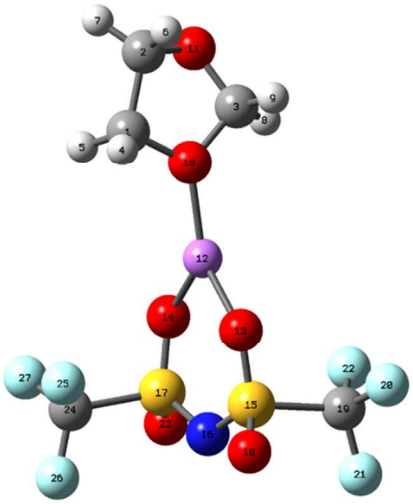	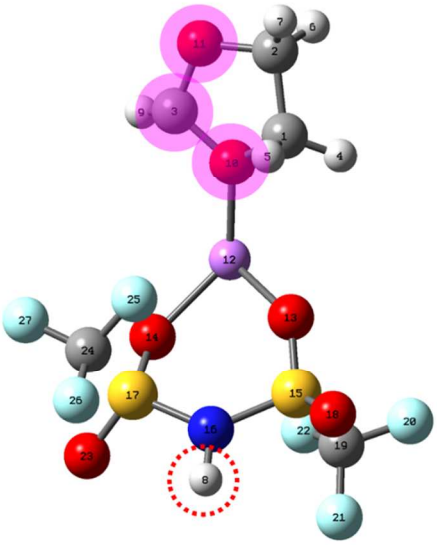

(d)	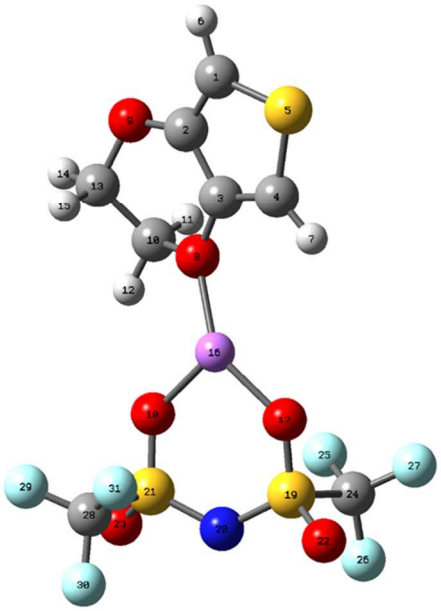	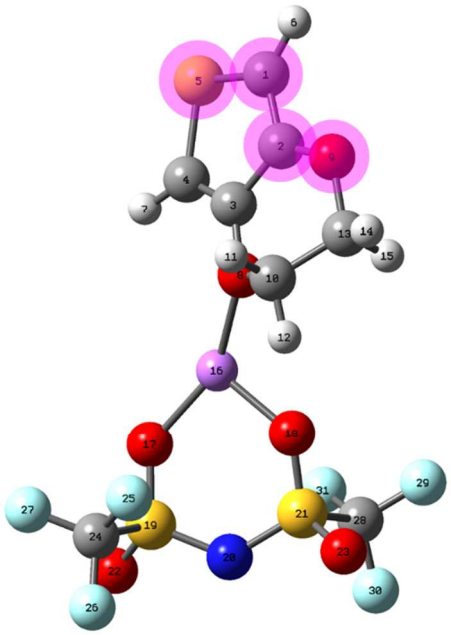
(e)	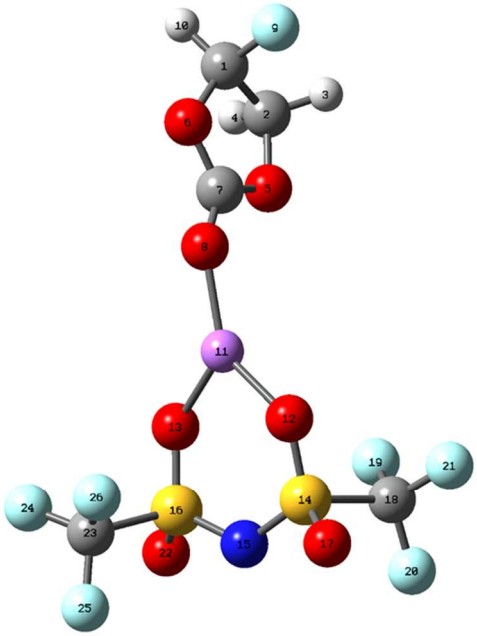	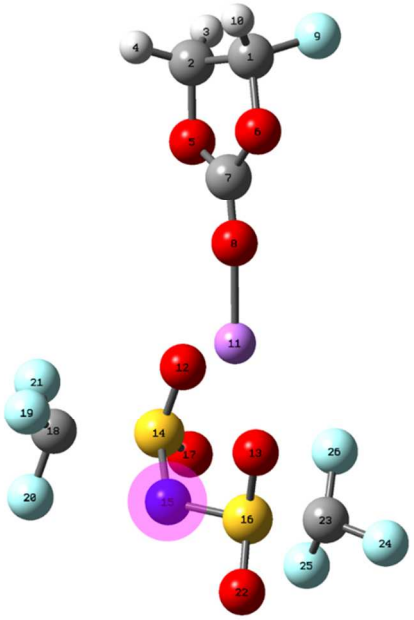

(f)	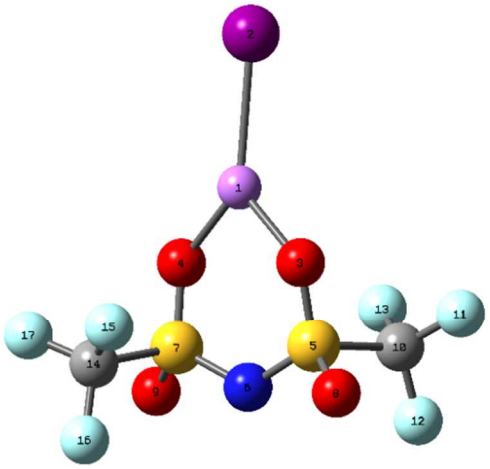	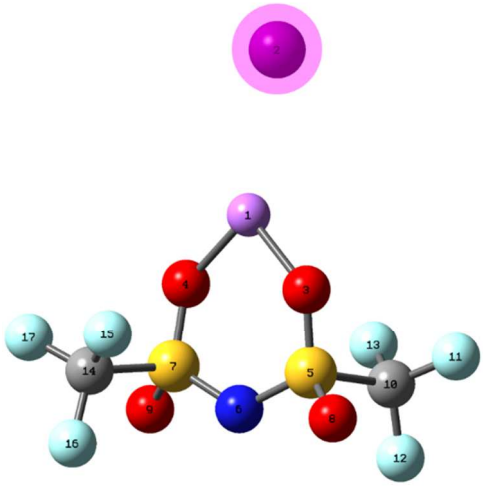
(g)	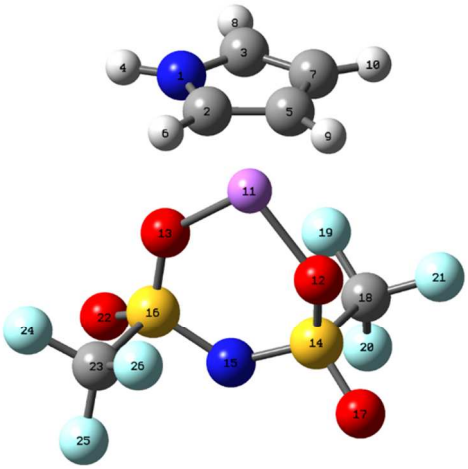	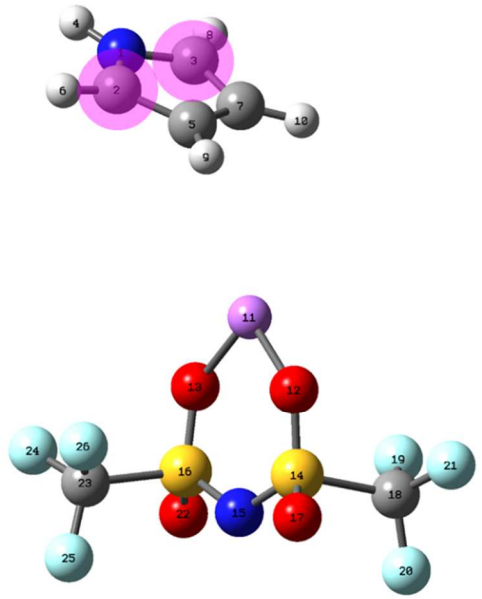

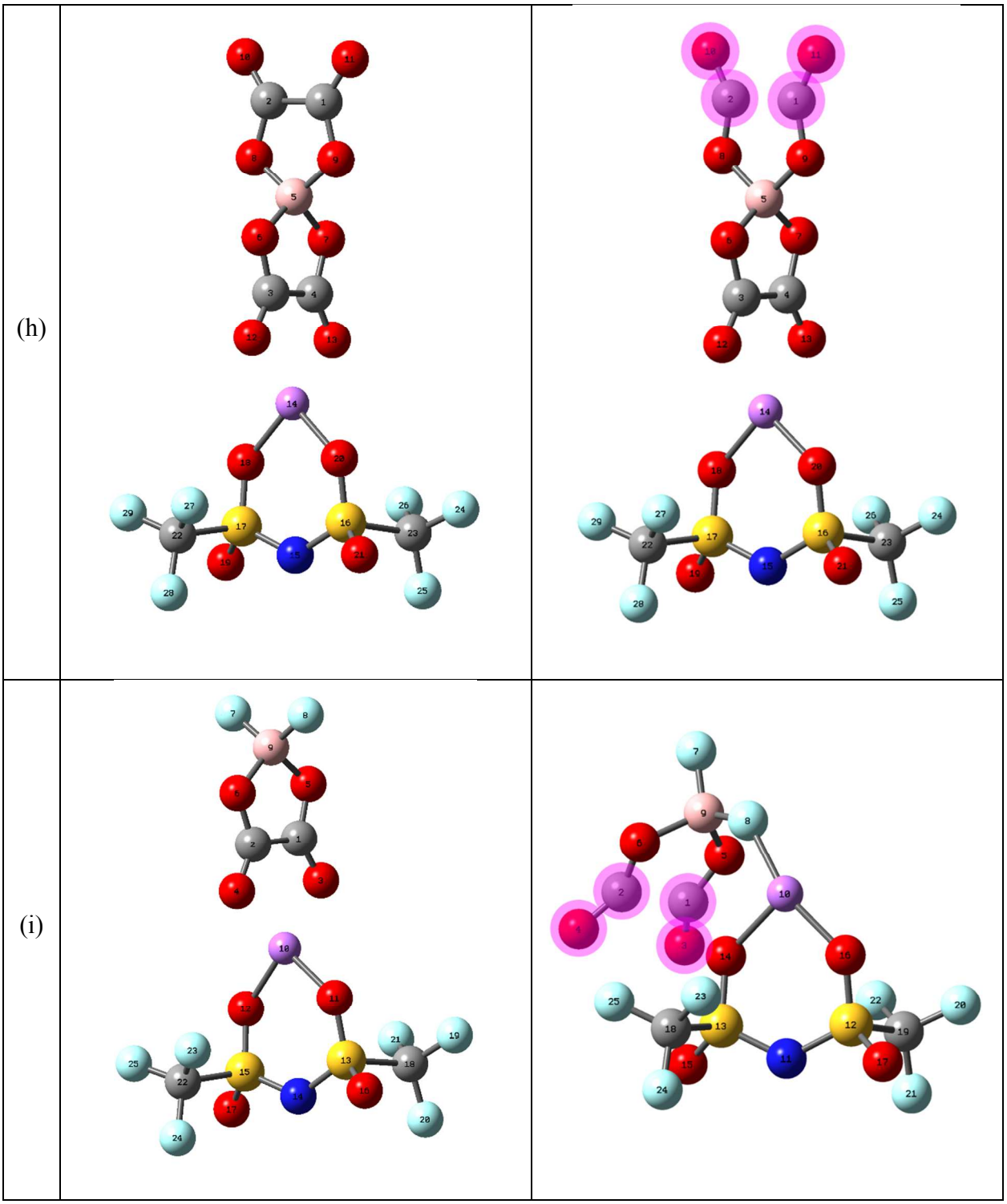

Figure 5. Optimized Geometries of Complexes of Solvents and Additives with LiTFSI both in the Initial and Oxidized States in the Solution Phase. (White, violet, peach, grey, blue, red, cyan, and yellow colors represent H, Li, B, C, N, O, F, and S atoms, respectively. The atoms with

significant positive spin densities by oxidation are highlighted in magenta, and H atoms circled in red are transferred to TFSI-.)

3.5. Oxidation Potentials of Complexes with S_8

In order to model the effect of the sulfur-carbon (S/C) cathode materials, the complexes of electrolyte molecules with S_8 and pyrene are considered in this section and in the next section, respectively. There are two opposite views on the role of metal oxide cathode materials in the oxidative decomposition of electrolyte molecules at much lower voltages than the potentials reported using glassy carbon electrodes, platinum electrodes and so on in Li-ion batteries; (1) catalyst for the electrolyte decomposition,[72-73] and (2) source of reactive oxygen to react with electrolyte, leading to the decomposition and gas evolution.[74-75] In Li/S batteries, however, there is no report yet that investigates the effect of sulfur and/or S/C composite cathode materials on the oxidative decomposition of electrolyte. Optimized geometries of electrolyte molecular complexes with S_8 are displayed in Figure 6, and CM5 charges and spin densities are listed in Table S4.

DME_ttt, and DME_tgt, and DOL complexes with S_8 have oxidation potentials of 5.34 V and 5.22 V, which is slightly enhanced from those of isolated DME_ttt and DME_tgt by 1.5 % and 1.2 %, respectively. Because DME_ttt and DME_tgt have slightly higher HOMO energies (-0.298 hartree and -0.293 hartree) than S_8 (-0.302 hartree), they are expected to be oxidized in complexes, and it is also confirmed by the locations of positive spin densities as shown in Figures 6a-b, and Table S4. However, the locations of HOMOs of DME_ttt/S_8 and DME_tgt/S_8 are a little inconsistent with the oxidation trends. The delocalization of HOMOs over the whole complexes is reasonable because of the negligible differences of HOMO electrons between

DME_ttt and S_8, and between DME_tgt and S_8. However, atomic orbitals on S atoms in S8 have higher coefficients than those in DME_ttt and DME_tgt, which indicates that HOMO electrons are distributed on S_8 more than on DME_ttt and DME_tgt, and HOMO electrons on S_8 are more susceptible to oxidation than those on DME_ttt and DME_tgt. Comparing electronegativities of O and S atoms, O atom has a higher electronegativity, 3.50, than S atom, 2.44,[76] which indicates that the O atom attracts electrons more easily than S atoms. Then, an electron in S_8 is removed by oxidation preferentially, compared to that in DME_ttt and DME_tgt, and an arrangement of electrons takes place. In our calculations, the optimized geometries of DME_ttt/S_8 and DME_tgt/S_8 complexes in the initial state are also employed for the oxidized state geometry optimizations, and the optimized geometries have not only higher zero-point-energy-corrected potential energies (9.5 kcal/mol and 7.8 kcal/mol for DME_ ttt/S_8 and DME_tgt/S_8, respectively) but also higher free energies (9.7 kcal/mol and 9.5 kcal/mol for DME_ ttt/S_8 and DME_tgt/S_8, respectively) than the optimized geometries for the oxidized states, displayed in Figures 5a-b. In addition, positive spin densities are located mostly on S_8. Therefore, there exist intermediates of the one-electron oxidation reactions in these complexes, where S_8 loses an electron by oxidation.

The oxidation potential of DOL/S_8 complex is calculated to be 5.56 V. HOMO energies of DOL (-0.304 hartree) and S_8 (-0.302 hartree) are very close, but HOMO is located mostly on S_8 as shown in Figure S3. However, positive spin densities are located both on DOL and on S_8 as displayed in Figure 6c and Table S4, which means that both DOL and S_8 are oxidized. The CM5 charges also show this oxidation trend; the charges of the DOL/S_8 complex change from 0.01e/-0.01e to 0.59e/0.41e, where both DOL and S_8 have positively increased charges by oxidation. The total spin density on DOL is 0.71, and that on S_8 is 0.29, which indicates that DOL has a higher unpaired electron density than S_8.

The FSI^-/S_8 complex has an oxidation potential of 5.36 V, and this is by the oxidation of S_8 from the HOMO location in the initial state and spin densities in the oxidized state. (Figure S4 and Table S4) In addition, the HOMO energy of S_8 (-0.30 Hartree) is higher than that of FSI^- (-0.32 hartree), which indicates that the HOMO electron of S_8 is more susceptible to oxidation. The $TFSI^-/S_8$ complex has the oxidation potential of 5.41 V, but oxidations of both complexes are different because of the similar HOMO energy level of $TFSI^-$ (-0.31 Hartree) compared to that of S_8. Although the HOMOs are located on S_8 in both complexes as shown in Figures S4-S5, spin density distributions in both complexes have a discrepancy, where spin densities are distributed only on S_8 in FSI^-/S_8 complex, but spin densities are distributed both on $TFSI^-$ and on S_8 in $TFSI^-/S_8$ complex. (Figures 6d-e) This difference is also reflected in charge changes. In the FSI^-/S_8 complex, FSI^- has a charge change from -0.96e to -0.86 while S_8 changes charges from -0.04e to 0.86e. In the $TFSI^-/S_8$ complex, however, $TFSI^-$ has a larger charge change than FSI^- from -0.96e to -0.62e, which indicates that $TFSI^-$ is more oxidized than FSI^-.

The oxidation potential of I^-/S_8 complex is 3.39 V, which is lower than that of isolated I^- only by 0.9 %. HOMO is located on I^- as in Figure S8, and the positive spin density is also located on I^- as in Figure 6f and Table S4. The pyrrole/S_8 complex also has a slightly reduced oxidation potential of 4.37 V, compared to the oxidation potential of the isolated pyrrole, 4.43 V. Pyrrole also has a HOMO electron on it, and the positive spin density is also located on pyrrole in the oxidized state. (Figure S9, Figure 6g, and Table S4) Because both I^- and pyrrole have much lower HOMO energy levels, -0.22 Hartree and 0.25 Hartree, respectively, than S_8, -0.30 Hartree, their HOMO electrons are more prone to be removed by oxidation than those of S_8.

Complexation of electrolyte molecules with S_8 does not show reductions in oxidation potentials within the operating voltage of Li/S batteries as shown above. These calculations are

intended to model the effect of the solid-state sulfur electrode on changes in oxidation potentials of electrolyte molecules; however, S_8 is also considered in the solution phase, and the S_8 complex is not an appropriate model to mimic the oxidation reaction of electrolyte molecules on the sulfur cathode material.

	Initial State	Oxidized State
(a)	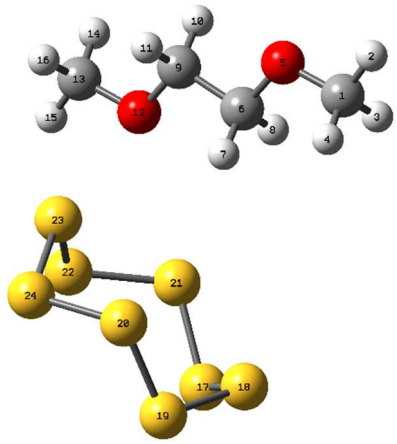	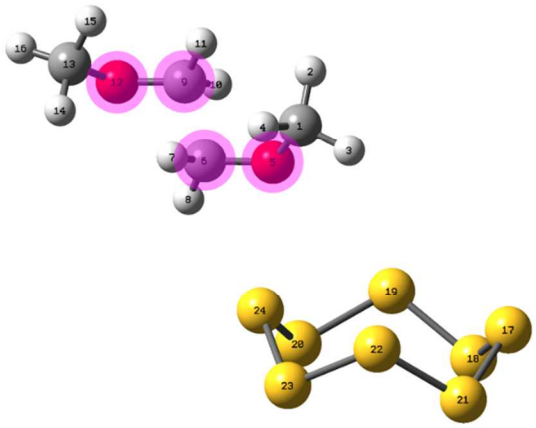

(b)	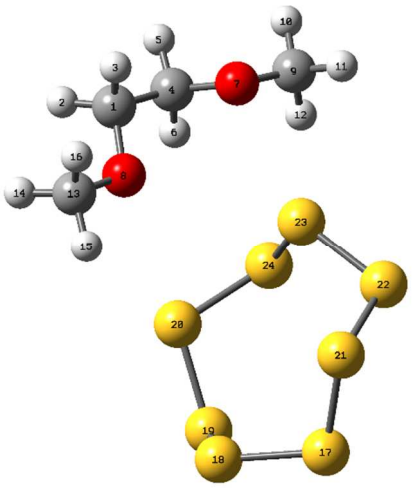	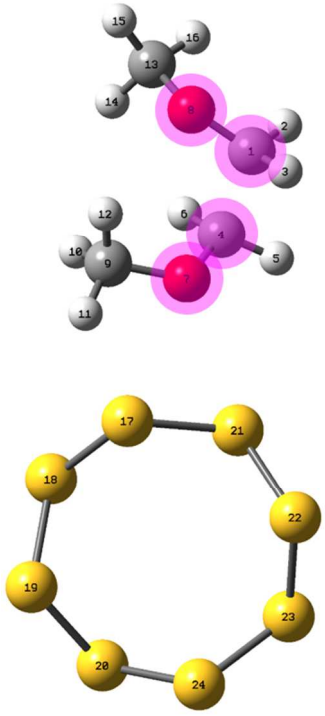
(c)	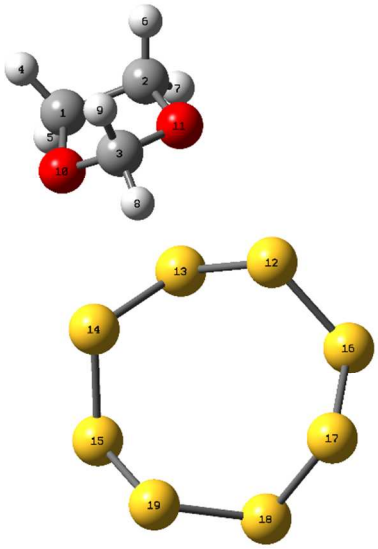	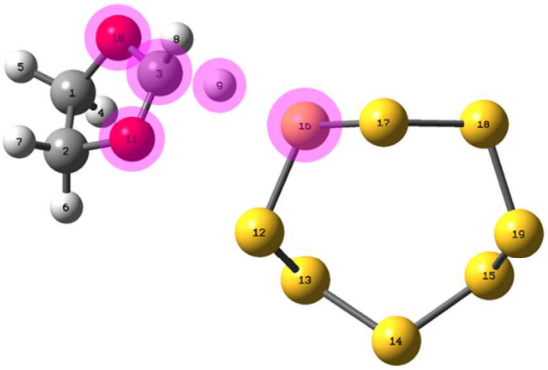

(d)	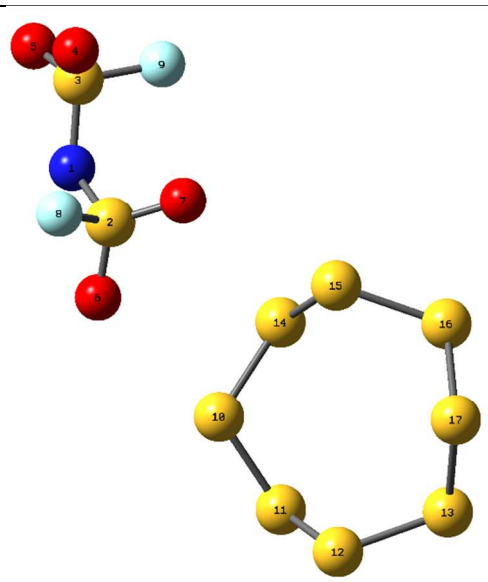	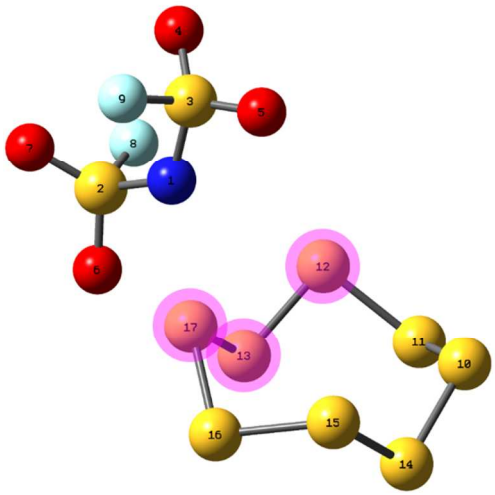
(e)	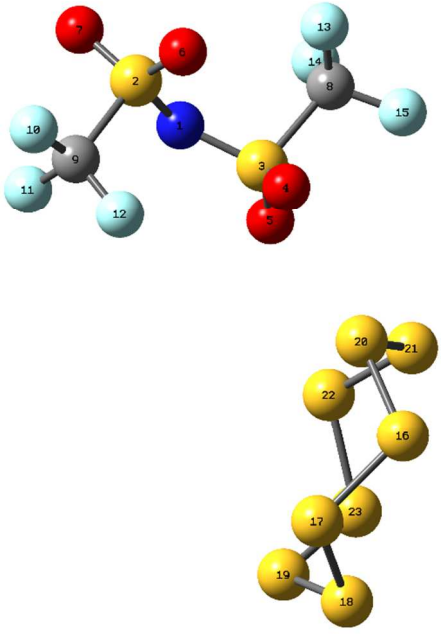	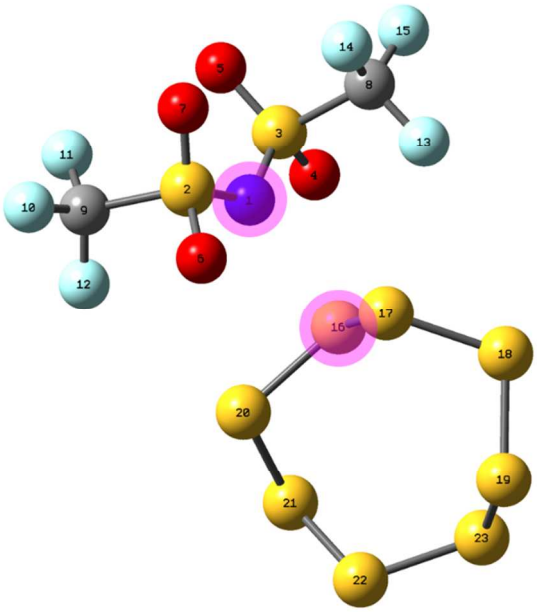

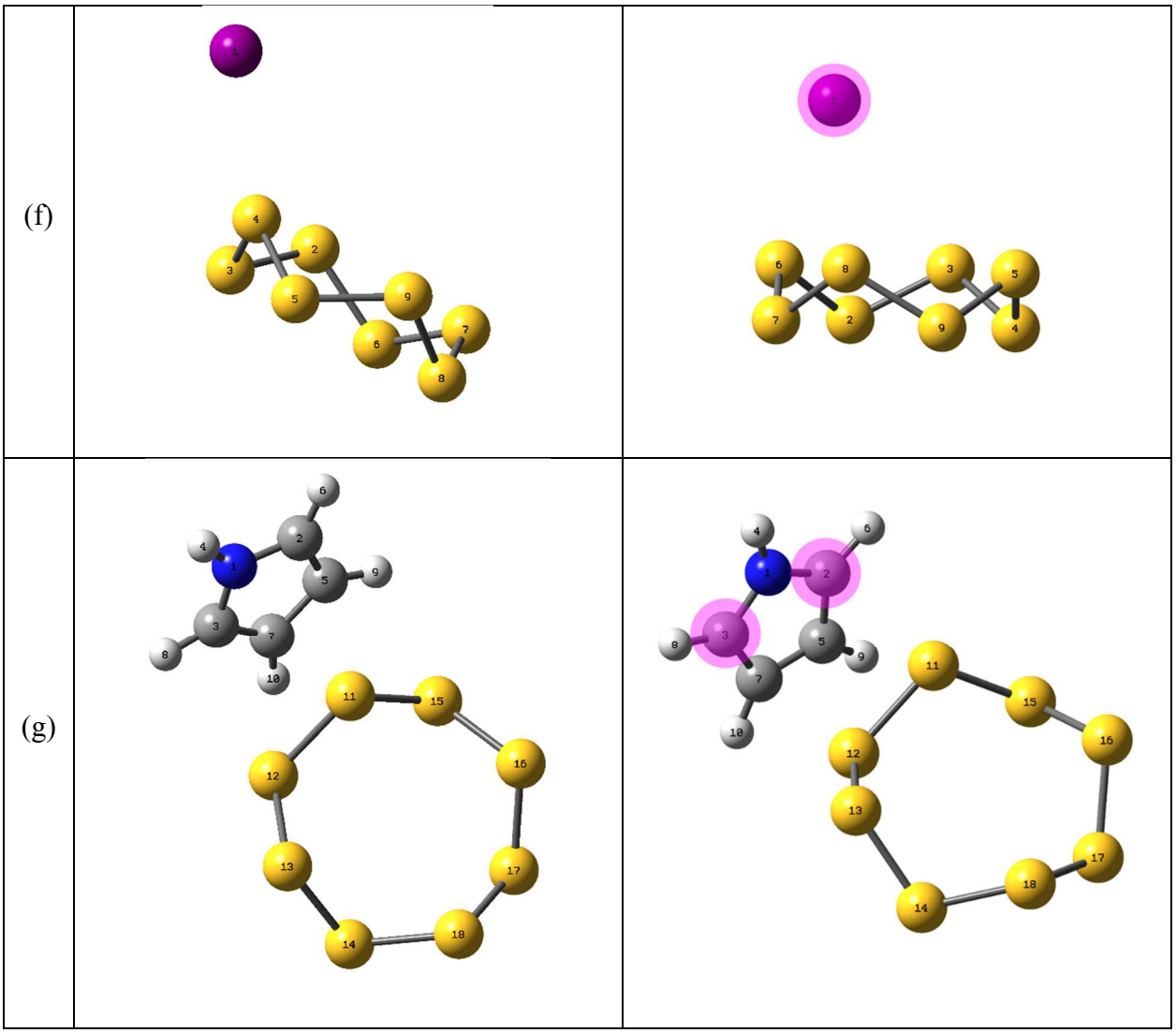

Figure 6. Optimized Geometries of Complexes of Solvents and Additives with S_8 both in the Initial and Oxidized States in the Solution Phase. (White, grey, blue, red, cyan, and yellow colors represent H, C, N, O, F, and S atoms, respectively, and the atoms with significant positive spin densities by oxidation are highlighted in magenta.)

3.6. Oxidation Potentials of Complexes with Pyrene

In this section, the complexes with pyrene are taken as a model compound for carbon composite cathode materials in Li/S batteries. In complexes with S_8, electrolyte molecules are mainly oxidized except that S_8 is oxidized in complexes with anions like FSI^- and $TFSI^-$.

However, the electrolyte complexes with pyrene have a different trend from the complexes with S_8 because of a higher HOMO energy of pyrene (-0.23 hartree) than electrolyte molecules in this study.

DME_ttt/pyrene, DME_tgt/pyrene, and DOL/pyrene complexes have oxidation potentials of 4.11 V, 4.33 V, and 4.26 V, respectively. Because the HOMO energy of pyrene is higher than those of DME_ttt (-0.30 hartree), DME_tgt (-0.29 hartree), and DOL (-0.30 hartree), pyrene is expected to be oxidized in complexes. HOMO location and spin densities are also consistent with this prediction as shown in Figures S1-S3, Figures 7a-c, and Table S5.

Oxidation potentials of FSI^-/pyrene and $TFSI^-$/pyrene complexes are obtained to 3.91 V and 4.01 V, respectively, which is lower than those of solvent/pyrene complexes above. In solvent/pyrene complexes, charges for solvent molecules and pyrene change from 0.02e/-0.02e, 0.05e/-0.05e, and 0.00e/0.00e to 0.04e/0.96e, -0.03e/1.03e, and 0.05e/0.95e for DME_ttt/pyrene, DME_tgt/pyrene, and DOL/pyrene complexes, respectively, where charges of solvent molecules remain close to zero, but those of pyrene get close to 1.00e. In anion/pyrene complexes, however, charges of anion and pyrene in each complex change from -0.92e/-0.08e and -1.00e/0.00e to -0.91e/0.91e and -0.92e/0.92e for FSI^-/pyrene and $TFSI^-$/pyrene complexes, respectively, where positive charges on oxidized pyrene are stabilized by negative charges on anions in the oxidized state. HOMO locations (Figures S4-S5) and spin densities (Figures 7d-e and Table S5) have the same trend as in the solvent/pyrene complexes described above.

The I^-/pyrene complex has an inconsistency between the HOMO location and the oxidation trend. The HOMO energies of I^- (-0.22 hartree at BMK/LanL2DZdp) and pyrene (-0.23 hartree at BMK/cc-pVTZ) are quite similar; therefore, the HOMO electron is expected to be distributed over the whole complex, but a little more on I^- because of its slightly higher HOMO

energy than that of pyrene. In the oxidized state, a positive spin density is located on oxidized I•, (Figure 7f and Table S5) and partial charge of I^- also increased from -0.93e to -0.19e, which indicates that I^- is oxidized to I• in the I^-/pyrene complex. However, the HOMO is completely delocalized only over pyrene molecule as shown in Figure S8, which indicates that the HOMO electron on pyrene is more prone to be removed by oxidation than that on I^-. This inconsistency stems from the use of different basis sets for I^- and pyrene together with the use of ECP for I^-.

The pyrrole/pyrene complex has an oxidation potential of 4.11 V, and it arises from the oxidation of pyrene, based on the positive spin densities on pyrene as shown in Figure 7g and Table S5. HOMO energy level of pyrrole is -0.25 hartree, which is lower than that of pyrene, and this is consistent with the oxidation trend described above.

Overall, as shown for the S_8 complexes in the previous section, the complexation with pyrene does not dramatically lower oxidation potentials of electrolyte molecules to place them within the operating voltage range of Li/S batteries. It is possible to argue that it is because of the inability to model the solid state of S/C electrodes in our calculations, and further studies are necessary to confirm the trends.

	Initial State	Oxidized State

(a)	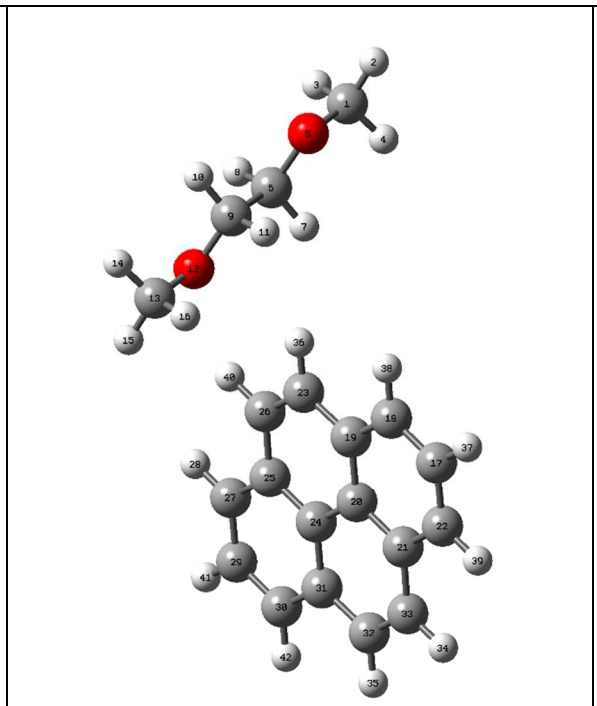	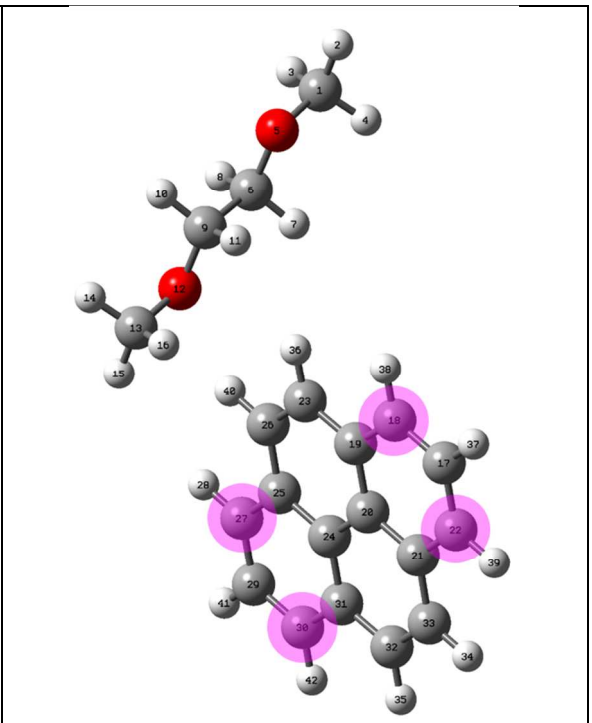
(b)	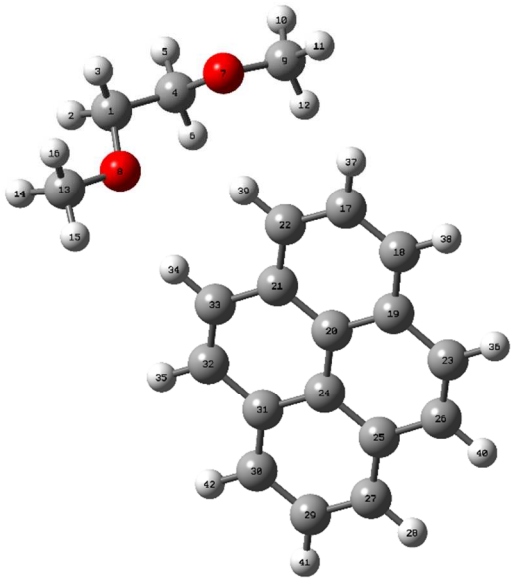	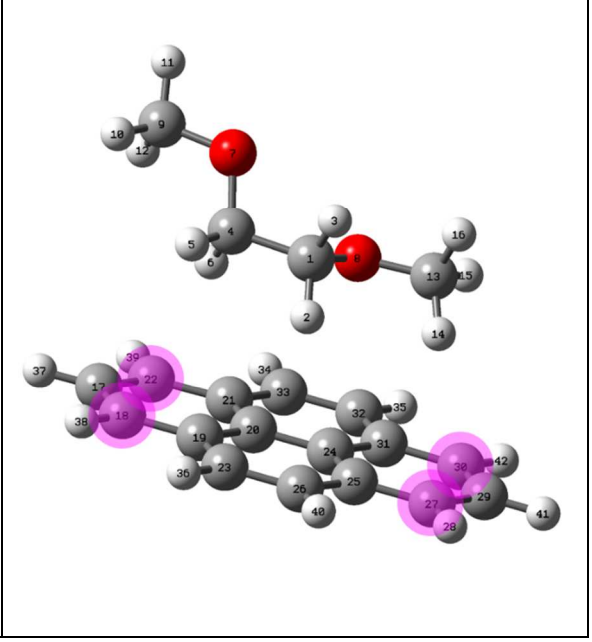

(c)	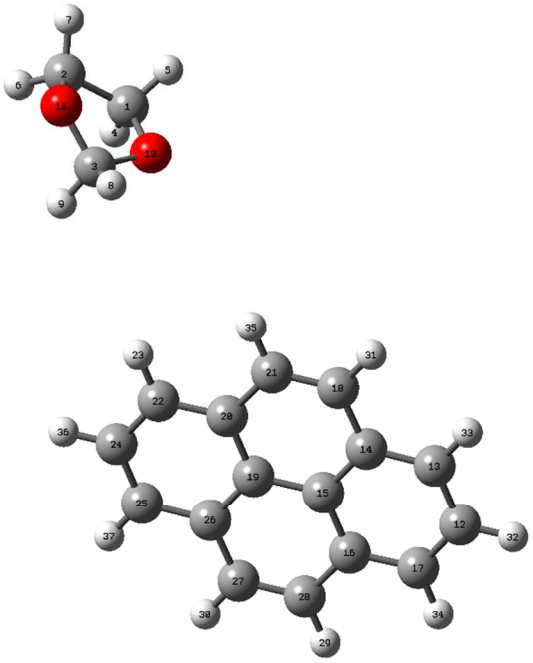	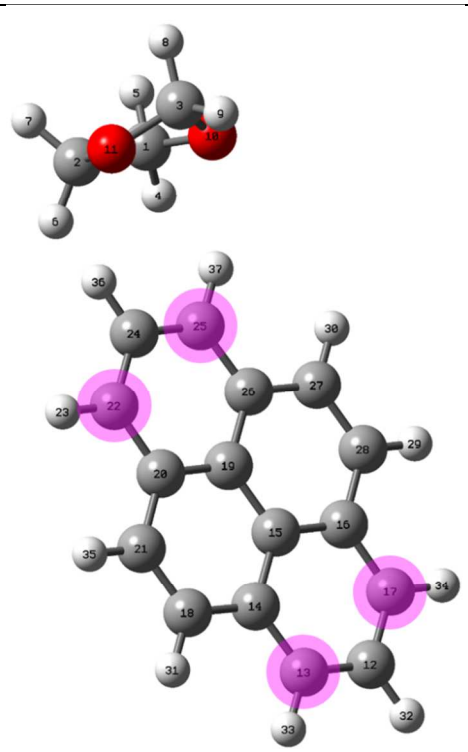
(d)	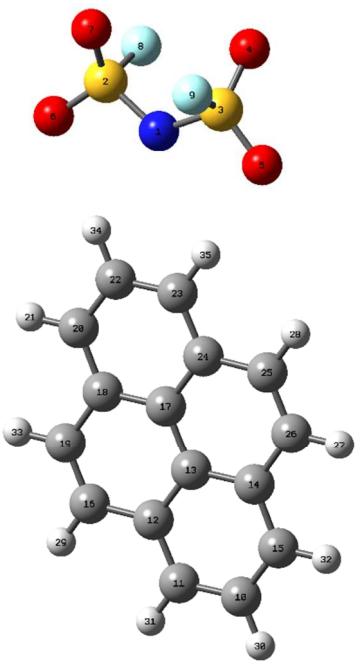	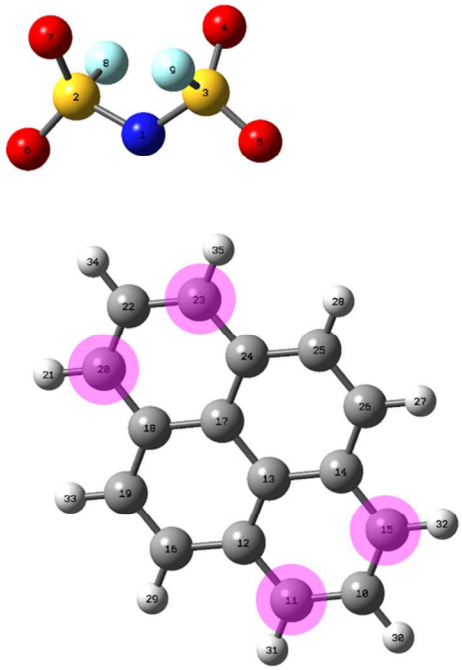

(e)	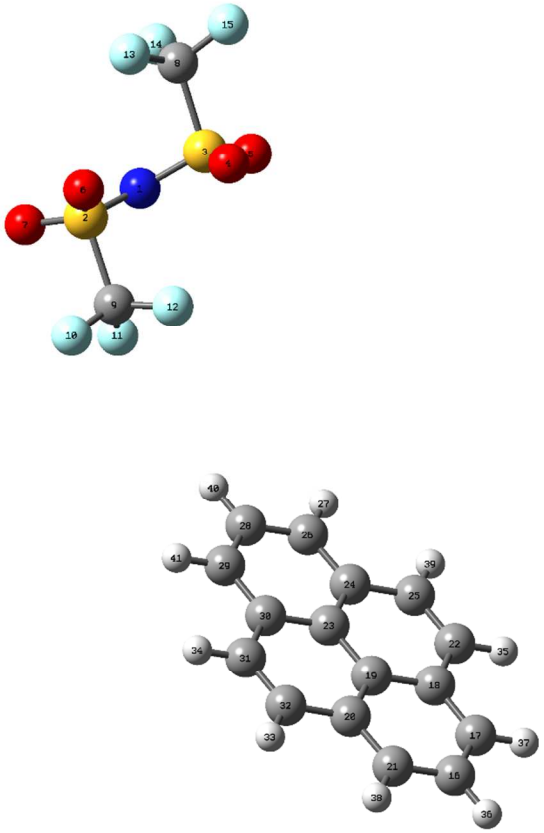	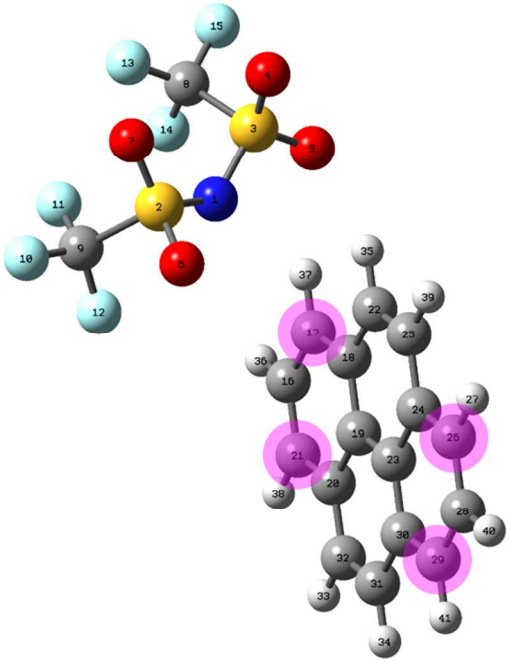
(f)	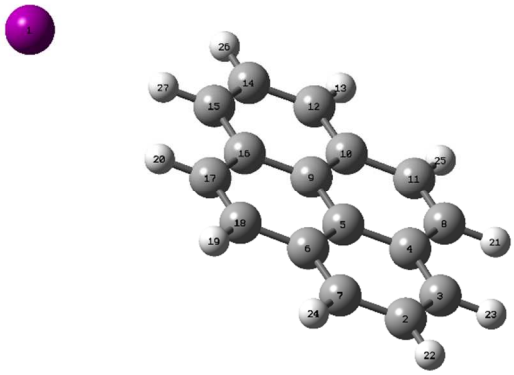	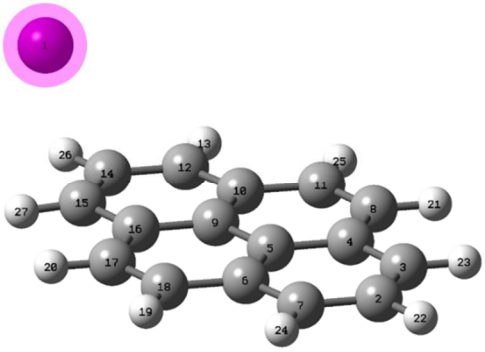

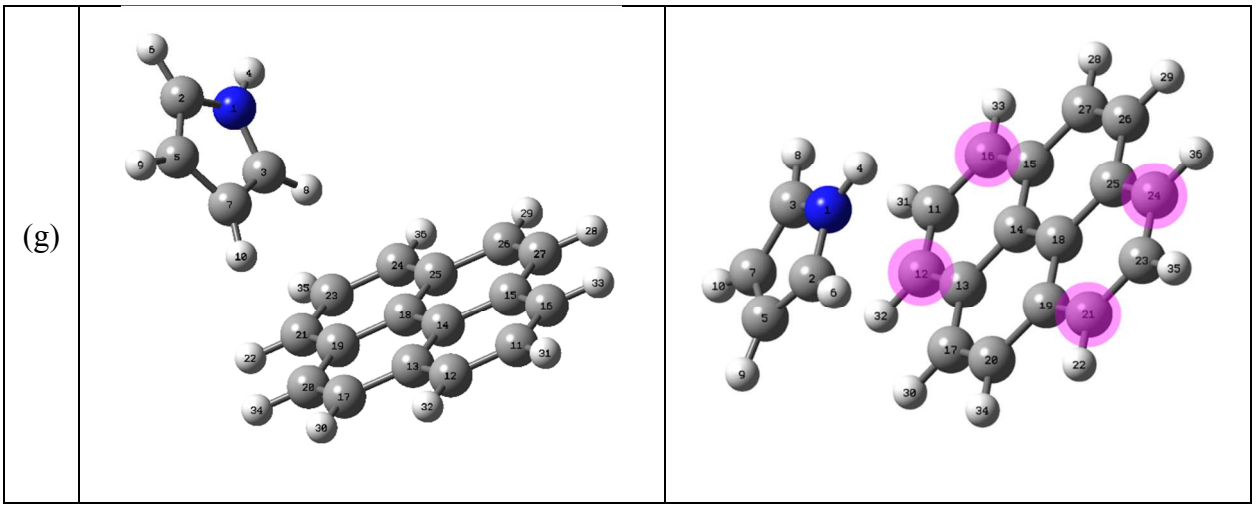

Figure 7. Optimized Geometries of Complexes of Solvents and Additives with Pyrene both in the Initial and Oxidized States in the Solution Phase. (White, grey, blue, red, cyan, and yellow colors represent H, C, N, O, F, and S atoms, respectively, and the atoms with significant positive spin densities by oxidation are highlighted in magenta.)

4. Conclusions

Oxidation potentials of electrolyte molecules are investigated using the DFT method not only in isolated molecules but also in complexes with Li^+, $TFSI^-$, LiTFSI, S_8, and pyrene. Isolated molecules have oxidation potentials lying above the operating voltage range of typical Li/S batteries from BMK/cc-pVTZ calculations (BMK/LanL2DZdp for I^-). Electrolyte solvents, including DME and DOL, tend to break bonds between C atoms in DME, and between the C atom, located between two O atoms, and H atoms in DOL by oxidation. $TFSI^-$ is also expected to release the CF_3 group in the oxidized state even though FSI^- is not. However, all Li/S battery additives, including EDOT, FEC, and pyrrole, remain in their geometries of the initial state. The Li-ion battery additives, BOB^- and $DFOB^-$, are also predicted to evolve CO_2 by oxidation. By complexation of electrolyte molecules, oxidation potentials change with counter species. Li^+ improves the stability of electrolyte molecules against oxidation, increasing oxidation potentials

by 10.4 % through 30.0 % from those of isolated molecules, and electrolyte molecules are oxidized in the Li^+ complexes. However, it is found that the Li salt anion, $TFSI^-$, lowers oxidation potential of electrolyte molecules by 4.7 % through 21.1 % by electrostatic stabilization while $TFSI^-$ is oxidized in the FEC/$TFSI^-$ complex. The proton transfer is critical in the solvent/$TFSI^-$ complexes in lowering oxidation potentials while the electrostatic stabilization by $TFSI^-$ play a role in additives/$TFSI^-$ complexes. Although the explicit existence of $TFSI^-$ helps reducing oxidation potentials, the reduced oxidation potentials are still out of the operating voltage range of Li/S batteries. In this study, only one $TFSI^-$ is added to the system, and the addition of more $TFSI^-$ can lower the oxidation potentials even more. Oxidation potentials of the complexes with LiTFSI are located between those of the isolated systems and complexes with Li^+, while $TFSI^-$ is also oxidized in the FEC/LiTFSI complex. Just as discussed in the complexes with $TFSI^-$, the proton transfer and the electrostatic stabilization play a role in the decrease in oxidation potential, compared to the complexes with Li^+. Complexes with S_8 and pyrene are also investigated to model the effect of sulfur and/or S/C composite cathode materials on the variation of oxidation potentials of electrolyte molecules. Electrolyte solvent molecules and additives are observed to be oxidized in complexes with S_8 with negligible changes in oxidation potentials by less than 2.0 % while S_8 is mainly oxidized in complexes with Li salt anions. Complexes with pyrene display oxidation of pyrene, not of electrolyte molecules while I^- is oxidized in the I^- /pyrene complex. However, the I^-/pyrene complex still has a higher oxidation potential than the operating voltage of Li/S batteries. Comparing the real battery cell system and the current models in S_8 and pyrene complexes, S_8 and pyrene have a different phase in this study from that in the real system; S_8 and pyrene are all solids in the latter, but they are in the solution phase in

the former. Therefore, complexes with S_8 and pyrene in the current study may be less appropriate to model the effect of sulfur and/or S/C composite electrode.

From the calculations of oxidation potentials of electrolyte molecules in Li/S batteries, the formation of a passivation layer on the cathode surface by oxidative decomposition of electrolyte additives hardly looks effective within the operating voltage range of Li/S batteries. In Li-ion batteries, the metal oxide cathode material can serve as a catalyst for oxidative decomposition of electrolyte molecules;[72-73] however, the sulfur cathode and the S/C composite cathode electrode have no such catalytic ability for the oxidative decomposition of electrolyte molecules. In order to mimic the reactions between cathode electrode and electrolyte molecules in Li/S batteries, electrode/electrolyte interface systems should be considered in calculating oxidation potentials and in modeling oxidative decomposition reactions of electrolyte systems. Passerini and co-workers also studied the effect of dissolved oxygen in dry air on the stability of electrolyte in Li/S batteries.[77] Therefore, the contamination and impurities present in the electrolyte should also be considered for oxidative decomposition reactions of electrolyte molecules in future work. In this study, only combinations of two different species are considered. In the real battery cell, however, there exist a variety of combinations of electrolyte species. Moreover, the continuum solvation model cannot properly describe the explicit interactions between electrolyte molecules and solvent molecules, which may affect oxidation potential trends. Therefore, it is useful to include at least the first solvation shell. In addition, oxidative decomposition of electrolyte is also expected when operated under abuse conditions such as a higher-voltage operation and an overcharge of a cell. However, adding all these effects would result in improved models at expenses of a substantial increase in the computational cost even using DFT methods.

Acknowledgements: This work was supported by the Assistant Secretary for Energy Efficiency and Renewable Energy, Office of Vehicle Technologies of the U.S. Department of Energy under Contract No. DE-EE0007766 under the Advanced Battery Materials Research (BMR) Program. Supercomputer resources from Texas A&M University High Performance Computer Center and Texas Advanced Computing Center (TACC) are gratefully acknowledged.

References

1. Anderman, M. *The xEV Industry Insider Report*; 2017.
2. EV Battery Goals. http://www.uscar.org/guest/article_view.php?articles_id=85.
3. Manthiram, A.; Chung, S. H.; Zu, C., Lithium–Sulfur Batteries: Progress and Prospects. *Advanced Materials* **2015,** *27* (12), 1980-2006.
4. Manthiram, A.; Fu, Y.; Chung, S.-H.; Zu, C.; Su, Y.-S., Rechargeable Lithium–Sulfur Batteries. *Chemical Reviews* **2014,** *114* (23), 11751-11787.
5. Abouimrane, A.; Odom, S. A.; Tavassol, H.; Schulmerich, M. V.; Wu, H.; Bhargava, R.; Gewirth, A. A.; Moore, J. S.; Amine, K., 3-Hexylthiophene as a Stabilizing Additive for High Voltage Cathodes in Lithium-Ion Batteries. *Journal of The Electrochemical Society* **2013,** *160* (2), A268-A271.
6. Kang, Y.-S.; Yoon, T.; Mun, J.; Park, M. S.; Song, I.-Y.; Benayad, A.; Oh, S. M., Effective passivation of a high-voltage positive electrode by 5-hydroxy-1H-indazole additives. *Journal of Materials Chemistry A* **2014,** *2* (35), 14628-14633.
7. Yang, J.; Zhao, P.; Shang, Y.; Wang, L.; He, X.; Fang, M.; Wang, J., Improvement in High-voltage Performance of Lithium-ion Batteries Using Bismaleimide as an Electrolyte Additive. *Electrochimica Acta* **2014,** *121*, 264-269.
8. Yang, L.; Lucht, B. L., Inhibition of Electrolyte Oxidation in Lithium Ion Batteries with Electrolyte Additives. *Electrochemical and Solid-State Letters* **2009,** *12* (12), A229-A231.
9. Xu, M.; Lu, D.; Garsuch, A.; Lucht, B. L., Improved Performance of LiNi0.5Mn1.5O4 Cathodes with Electrolytes Containing Dimethylmethylphosphonate (DMMP). *Journal of The Electrochemical Society* **2012,** *159* (12), A2130-A2134.
10. Li, Y.; Lian, F.; Ma, L.; Liu, C.; Yang, L.; Sun, X.; Chou, K., Fluoroethylene Carbonate as Electrolyte Additive for Improving the electrochemical performances of High-Capacity Li1.16[Mn0.75Ni0.25]0.84O2 Material. *Electrochimica Acta* **2015,** *168*, 261-270.
11. Bouayad, H.; Wang, Z.; Dupré, N.; Dedryvère, R.; Foix, D.; Franger, S.; Martin, J. F.; Boutafa, L.; Patoux, S.; Gonbeau, D.; Guyomard, D., Improvement of Electrode/Electrolyte Interfaces in High-Voltage Spinel Lithium-Ion Batteries by Using Glutaric Anhydride as Electrolyte Additive. *The Journal of Physical Chemistry C* **2014,** *118* (9), 4634-4648.
12. von Cresce, A.; Xu, K., Electrolyte Additive in Support of 5 V Li Ion Chemistry. *Journal of The Electrochemical Society* **2011,** *158* (3), A337-A342.

13. Zuo, X.; Fan, C.; Liu, J.; Xiao, X.; Wu, J.; Nan, J., Lithium Tetrafluoroborate as an Electrolyte Additive to Improve the High Voltage Performance of Lithium-Ion Battery. *Journal of The Electrochemical Society* **2013,** *160* (8), A1199-A1204.
14. Dalavi, S.; Xu, M.; Knight, B.; Lucht, B. L., Effect of Added LiBOB on High Voltage (LiNi0.5Mn1.5O4) Spinel Cathodes. *Electrochemical and Solid-State Letters* **2011,** *15* (2), A28-A31.
15. Yang, L.; Markmaitree, T.; Lucht, B. L., Inorganic additives for passivation of high voltage cathode materials. *Journal of Power Sources* **2011,** *196* (4), 2251-2254.
16. Fu, M. H.; Huang, K. L.; Liu, S. Q.; Liu, J. S.; Li, Y. K., Lithium difluoro(oxalato)borate/ethylene carbonate+propylene carbonate+ethyl(methyl) carbonate electrolyte for LiMn2O4 cathode. *Journal of Power Sources* **2010,** *195* (3), 862-866.
17. Xu, M.; Zhou, L.; Dong, Y.; Chen, Y.; Demeaux, J.; MacIntosh, A. D.; Garsuch, A.; Lucht, B. L., Development of novel lithium borate additives for designed surface modification of high voltage LiNi0.5Mn1.5O4 cathodes. *Energy & Environmental Science* **2016,** *9* (4), 1308-1319.
18. Zuo, X.; Fan, C.; Xiao, X.; Liu, J.; Nan, J., High-voltage performance of LiCoO2/graphite batteries with methylene methanedisulfonate as electrolyte additive. *Journal of Power Sources* **2012,** *219*, 94-99.
19. Li, B.; Wang, Y.; Tu, W.; Wang, Z.; Xu, M.; Xing, L.; Li, W., Improving cyclic stability of lithium nickel manganese oxide cathode for high voltage lithium ion battery by modifying electrode/electrolyte interface with electrolyte additive. *Electrochimica Acta* **2014,** *147*, 636-642.
20. Dong, P.; Wang, D.; Yao, Y.; Li, X.; Zhang, Y.; Ru, J.; Ren, T., Stabilizing interface layer of LiNi0.5Co0.2Mn0.3O2 cathode materials under high voltage using p-toluenesulfonyl isocyanate as film forming additive. *Journal of Power Sources* **2017,** *344*, 111-118.
21. Xu, H. Y.; Xie, S.; Wang, Q. Y.; Yao, X. L.; Wang, Q. S.; Chen, C. H., Electrolyte additive trimethyl phosphite for improving electrochemical performance and thermal stability of LiCoO2 cathode. *Electrochimica Acta* **2006,** *52* (2), 636-642.
22. Zuo, X.; Fan, C.; Liu, J.; Xiao, X.; Wu, J.; Nan, J., Effect of tris(trimethylsilyl)borate on the high voltage capacity retention of LiNi0.5Co0.2Mn0.3O2/graphite cells. *Journal of Power Sources* **2013,** *229*, 308-312.
23. Yan, G.; Li, X.; Wang, Z.; Guo, H.; Wang, C., Tris(trimethylsilyl)phosphate: A film-forming additive for high voltage cathode material in lithium-ion batteries. *Journal of Power Sources* **2014,** *248*, 1306-1311.
24. Song, Y.-M.; Han, J.-G.; Park, S.; Lee, K. T.; Choi, N.-S., A multifunctional phosphite-containing electrolyte for 5 V-class LiNi0.5Mn1.5O4 cathodes with superior electrochemical performance. *Journal of Materials Chemistry A* **2014,** *2* (25), 9506-9513.
25. Xu, J.; Hu, Y.; liu, T.; Wu, X., Improvement of cycle stability for high-voltage lithium-ion batteries by in-situ growth of SEI film on cathode. *Nano Energy* **2014,** *5*, 67-73.
26. Kam, D.; Kim, K.; Kim, H.-S.; Liu, H. K., Studies on film formation on cathodes using pyrazole derivatives as electrolyte additives in the Li-ion battery. *Electrochemistry Communications* **2009,** *11* (8), 1657-1660.
27. Kim, K.; Kim, Y.; Oh, E.-S.; Shin, H.-C., The role of fluoride in protecting LiNi0.5Mn1.5O4 electrodes against high temperature degradation. *Electrochimica Acta* **2013,** *114*, 387-393.
28. Song, J.; Noh, H.; Lee, H.; Lee, J.-N.; Lee, D. J.; Lee, Y.; Kim, C. H.; Lee, Y. M.; Park, J.-K.; Kim, H.-T., Polysulfide rejection layer from alpha-lipoic acid for high performance lithium-sulfur battery. *Journal of Materials Chemistry A* **2015,** *3* (1), 323-330.
29. Song, J.; Noh, H.; Lee, J.; Nah, I.-W.; Cho, W.-I.; Kim, H.-T., In situ coating of Poly(3,4-ethylenedioxythiophene) on sulfur cathode for high performance lithium–sulfur batteries. *Journal of Power Sources* **2016,** *332*, 72-78.
30. Yang, W.; Yang, W.; Song, A.; Gao, L.; Sun, G.; Shao, G., Pyrrole as a promising electrolyte additive to trap polysulfides for lithium-sulfur batteries. *Journal of Power Sources* **2017,** *348*, 175-182.

31. Wu, F.; Lee, J. T.; Nitta, N.; Kim, H.; Borodin, O.; Yushin, G., Lithium Iodide as a Promising Electrolyte Additive for Lithium–Sulfur Batteries: Mechanisms of Performance Enhancement. *Advanced Materials* **2015,** *27* (1), 101-108.
32. Lee, J. T.; Eom, K.; Wu, F.; Kim, H.; Lee, D. C.; Zdyrko, B.; Yushin, G., Enhancing the Stability of Sulfur Cathodes in Li–S Cells via in Situ Formation of a Solid Electrolyte Layer. *ACS Energy Letters* **2016,** *1* (2), 373-379.
33. Becke, A. D., Density-functional thermochemistry. III. The role of exact exchange. *The Journal of Chemical Physics* **1993,** *98* (7), 5648-5652.
34. Burke, K.; Perdew, J. P.; Wang, Y., Derivation of a Generalized Gradient Approximation: The PW91 Density Functional. In *Electronic Density Functional Theory: Recent Progress and New Directions*, Dobson, J. F.; Vignale, G.; Das, M. P., Eds. Springer US: Boston, MA, 1998; pp 81-111.
35. Boese, A. D.; Martin, J. M. L., Development of density functionals for thermochemical kinetics. *The Journal of Chemical Physics* **2004,** *121* (8), 3405-3416.
36. Zhao, Y.; Truhlar, D. G., The M06 suite of density functionals for main group thermochemistry, thermochemical kinetics, noncovalent interactions, excited states, and transition elements: two new functionals and systematic testing of four M06-class functionals and 12 other functionals. *Theoretical Chemistry Accounts* **2008,** *120* (1), 215-241.
37. McLean, A. D.; Chandler, G. S., Contracted Gaussian basis sets for molecular calculations. I. Second row atoms, Z=11–18. *The Journal of Chemical Physics* **1980,** *72* (10), 5639-5648.
38. Jr., T. H. D., Gaussian basis sets for use in correlated molecular calculations. I. The atoms boron through neon and hydrogen. *The Journal of Chemical Physics* **1989,** *90* (2), 1007-1023.
39. Kendall, R. A.; Jr., T. H. D.; Harrison, R. J., Electron affinities of the first-row atoms revisited. Systematic basis sets and wave functions. *The Journal of Chemical Physics* **1992,** *96* (9), 6796-6806.
40. Papajak, E.; Zheng, J.; Xu, X.; Leverentz, H. R.; Truhlar, D. G., Perspectives on Basis Sets Beautiful: Seasonal Plantings of Diffuse Basis Functions. *Journal of Chemical Theory and Computation* **2011,** *7* (10), 3027-3034.
41. Check, C. E.; Faust, T. O.; Bailey, J. M.; Wright, B. J.; Gilbert, T. M.; Sunderlin, L. S., Addition of Polarization and Diffuse Functions to the LANL2DZ Basis Set for P-Block Elements. *The Journal of Physical Chemistry A* **2001,** *105* (34), 8111-8116.
42. Schuchardt, K. L.; Didier, B. T.; Elsethagen, T.; Sun, L.; Gurumoorthi, V.; Chase, J.; Li, J.; Windus, T. L., Basis Set Exchange: A Community Database for Computational Sciences. *Journal of Chemical Information and Modeling* **2007,** *47* (3), 1045-1052.
43. Marenich, A. V.; Cramer, C. J.; Truhlar, D. G., Universal Solvation Model Based on Solute Electron Density and on a Continuum Model of the Solvent Defined by the Bulk Dielectric Constant and Atomic Surface Tensions. *The Journal of Physical Chemistry B* **2009,** *113* (18), 6378-6396.
44. Frisch, M. J.; Trucks, G. W.; Schlegel, H. B.; Scuseria, G. E.; Robb, M. A.; Cheeseman, J. R.; Scalmani, G.; Barone, V.; Petersson, G. A.; Nakatsuji, H.; Li, X.; Caricato, M.; Marenich, A.; Bloino, J.; Janesko, B. G.; Gomperts, R.; Mennucci, B.; Hratchian, H. P.; Ortiz, J. V.; Izmaylov, A. F.; Sonnenberg, J. L.; Williams-Young, D.; Ding, F.; Lipparini, F.; Egidi, F.; Goings, J.; Peng, B.; Petrone, A.; Henderson, T.; Ranasinghe, D.; Zakrzewski, V. G.; Gao, J.; Rega, N.; Zheng, G.; Liang, W.; Hada, M.; Ehara, M.; Toyota, K.; Fukuda, R.; Hasegawa, J.; Ishida, M.; Nakajima, T.; Honda, Y.; Kitao, O.; Nakai, H.; Vreven, T.; Throssell, K.; Montgomery, J., J. A.; Peralta, J. E.; Ogliaro, F.; Bearpark, M.; Heyd, J. J.; Brothers, E.; Kudin, K. N.; Staroverov, V. N.; Keith, T.; Kobayashi, R.; Normand, J.; Raghavachari, K.; Rendell, A.; Burant, J. C.; Iyengar, S. S.; Tomasi, J.; Cossi, M.; Millam, J. M.; Klene, M.; Adamo, C.; Cammi, R.; Ochterski, J. W.; Martin, R. L.; Morokuma, K.; Farkas, O.; Foresman, J. B.; Fox, D. J. *Gaussian 09*, Revision D.01; Gaussian, Inc: Wallingford CT, 2013.
45. BIOVIA, D. S. *Materials Studio*, 8.0.0.843; Dassault Système: San Diego, 2014.

46. Grimme, S.; Antony, J.; Ehrlich, S.; Krieg, H., A consistent and accurate ab initio parametrization of density functional dispersion correction (DFT-D) for the 94 elements H-Pu. *The Journal of Chemical Physics* **2010,** *132* (15), 154104.
47. Grimme, S.; Ehrlich, S.; Goerigk, L., Effect of the damping function in dispersion corrected density functional theory. *Journal of Computational Chemistry* **2011,** *32* (7), 1456-1465.
48. Borodin, O.; Behl, W.; Jow, T. R., Oxidative Stability and Initial Decomposition Reactions of Carbonate, Sulfone, and Alkyl Phosphate-Based Electrolytes. *The Journal of Physical Chemistry C* **2013,** *117* (17), 8661-8682.
49. Ossola, F.; Pistoia, G.; Seeber, R.; Ugo, P., Oxidation potentials of electrolyte solutions for lithium cells. *Electrochimica Acta* **1988,** *33* (1), 47-50.
50. Ue, M.; Takeda, M.; Takehara, M.; Mori, S., Electrochemical Properties of Quaternary Ammonium Salts for Electrochemical Capacitors. *Journal of The Electrochemical Society* **1997,** *144* (8), 2684-2688.
51. Han, H.-B.; Zhou, S.-S.; Zhang, D.-J.; Feng, S.-W.; Li, L.-F.; Liu, K.; Feng, W.-F.; Nie, J.; Li, H.; Huang, X.-J.; Armand, M.; Zhou, Z.-B., Lithium bis(fluorosulfonyl)imide (LiFSI) as conducting salt for nonaqueous liquid electrolytes for lithium-ion batteries: Physicochemical and electrochemical properties. *Journal of Power Sources* **2011,** *196* (7), 3623-3632.
52. Ue, M.; Murakami, A.; Nakamura, S., Anodic Stability of Several Anions Examined by Ab Initio Molecular Orbital and Density Functional Theories. *Journal of The Electrochemical Society* **2002,** *149* (12), A1572-A1577.
53. Lan, X.; Bencan, T.; Linbin, Y.; Kai, W.; Anastasia, C.; Yueyang, P.; Saixi, L.; Yonggao, X.; Z., C. G.; Zhaoping, L., Oxidation Decomposition Mechanism of Fluoroethylene Carbonate-Based Electrolytes for High-Voltage Lithium Ion Batteries: A DFT Calculation and Experimental Study. *ChemistrySelect* **2017,** *2* (24), 7353-7361.
54. Tabba, H. D.; Smith, K. M., Anodic oxidation potentials of substituted pyrroles: derivation and analysis of substituent partial potentials. *The Journal of Organic Chemistry* **1984,** *49* (11), 1870-1875.
55. Xu, W.; Angell, C. A., Weakly Coordinating Anions, and the Exceptional Conductivity of Their Nonaqueous Solutions. *Electrochemical and Solid-State Letters* **2001,** *4* (1), E1-E4.
56. Hu, M.; Wei, J.; Xing, L.; Zhou, Z., Effect of lithium difluoro(oxalate)borate (LiDFOB) additive on the performance of high-voltage lithium-ion batteries. *Journal of Applied Electrochemistry* **2012,** *42* (5), 291-296.
57. Hirshfeld, F. L., Bonded-atom fragments for describing molecular charge densities. *Theoretica chimica acta* **1977,** *44* (2), 129-138.
58. Marenich, A. V.; Jerome, S. V.; Cramer, C. J.; Truhlar, D. G., Charge Model 5: An Extension of Hirshfeld Population Analysis for the Accurate Description of Molecular Interactions in Gaseous and Condensed Phases. *Journal of Chemical Theory and Computation* **2012,** *8* (2), 527-541.
59. Zhang, X.; Pugh, J. K.; Ross, P. N., Computation of Thermodynamic Oxidation Potentials of Organic Solvents Using Density Functional Theory. *Journal of The Electrochemical Society* **2001,** *148* (5), E183-E188.
60. Trasatti, S., The absolute electrode potential: an explanatory note. *Pure & Applied Chemistry* **1986,** *58* (7), 955-966.
61. Tan, Y.; Ghandi, K., Kinetics and mechanism of pyrrole chemical polymerization. *Synthetic Metals* **2013,** *175*, 183-191.
62. Kaymaksiz, S.; Wilhelm, F.; Wachtler, M.; Wohlfahrt-Mehrens, M.; Hartnig, C.; Tschernych, I.; Wietelmann, U., Electrochemical stability of lithium salicylato-borates as electrolyte additives in Li-ion batteries. *Journal of Power Sources* **2013,** *239*, 659-669.

63. Wang, Y.; Xing, L.; Tang, X.; Li, X.; Li, W.; Li, B.; Huang, W.; Zhou, H.; Li, X., Oxidative stability and reaction mechanism of lithium bis(oxalate)borate as a cathode film-forming additive for lithium ion batteries. *RSC Advances* **2014,** *4* (63), 33301-33306.
64. Xu, M.; Tsiouvaras, N.; Garsuch, A.; Gasteiger, H. A.; Lucht, B. L., Generation of Cathode Passivation Films via Oxidation of Lithium Bis(oxalato) Borate on High Voltage Spinel (LiNi0.5Mn1.5O4). *The Journal of Physical Chemistry C* **2014,** *118* (14), 7363-7368.
65. Zhu, Y.; Li, Y.; Bettge, M.; Abraham, D. P., Positive Electrode Passivation by LiDFOB Electrolyte Additive in High-Capacity Lithium-Ion Cells. *Journal of The Electrochemical Society* **2012,** *159* (12), A2109-A2117.
66. Shkrob, I. A.; Zhu, Y.; Marin, T. W.; Abraham, D. P., Mechanistic Insight into the Protective Action of Bis(oxalato)borate and Difluoro(oxalate)borate Anions in Li-Ion Batteries. *The Journal of Physical Chemistry C* **2013,** *117* (45), 23750-23756.
67. Borodin, O.; Jow, T. R., Quantum Chemistry Studies of the Oxidative Stability of Carbonate, Sulfone and Sulfonate-Based Electrolytes Doped with BF4 -, PF6 - Anions. *ECS Transactions* **2011,** *33* (28), 77-84.
68. Xing, L.; Borodin, O.; Smith, G. D.; Li, W., Density Functional Theory Study of the Role of Anions on the Oxidative Decomposition Reaction of Propylene Carbonate. *The Journal of Physical Chemistry A* **2011,** *115* (47), 13896-13905.
69. Wang, Y.; Xing, L.; Li, W.; Bedrov, D., Why Do Sulfone-Based Electrolytes Show Stability at High Voltages? Insight from Density Functional Theory. *The Journal of Physical Chemistry Letters* **2013,** *4* (22), 3992-3999.
70. Qu, X.; Persson, K. A., Toward Accurate Modeling of the Effect of Ion-Pair Formation on Solute Redox Potential. *Journal of Chemical Theory and Computation* **2016,** *12* (9), 4501-4508.
71. Izutsu, K., *Electrochemistry in Nonaqueous Solutions*. 2nd ed.; Wiley-VCH: Germany, 2009.
72. Xu, K.; Ding, S. P.; Jow, T. R., Toward Reliable Values of Electrochemical Stability Limits for Electrolytes. *Journal of The Electrochemical Society* **1999,** *146* (11), 4172-4178.
73. Shkrob, I. A.; Abraham, D. P., Electrocatalysis Paradigm for Protection of Cathode Materials in High-Voltage Lithium-Ion Batteries. *The Journal of Physical Chemistry C* **2016,** *120* (28), 15119-15128.
74. Jung, R.; Metzger, M.; Maglia, F.; Stinner, C.; Gasteiger, H. A., Chemical versus Electrochemical Electrolyte Oxidation on NMC111, NMC622, NMC811, LNMO, and Conductive Carbon. *The Journal of Physical Chemistry Letters* **2017,** *8* (19), 4820-4825.
75. Jung, R.; Metzger, M.; Maglia, F.; Stinner, C.; Gasteiger, H. A., Oxygen Release and Its Effect on the Cycling Stability of LiNixMnyCozO2 (NMC) Cathode Materials for Li-Ion Batteries. *Journal of The Electrochemical Society* **2017,** *164* (7), A1361-A1377.
76. Little, E. J.; Jones, M. M., A complete table of electronegativities. *Journal of Chemical Education* **1960,** *37* (5), 231.
77. Lodovico, L.; Varzi, A.; Passerini, S., Radical Decomposition of Ether-Based Electrolytes for Li-S Batteries. *Journal of The Electrochemical Society* **2017,** *164* (9), A1812-A1819.

Table of Contents Entry

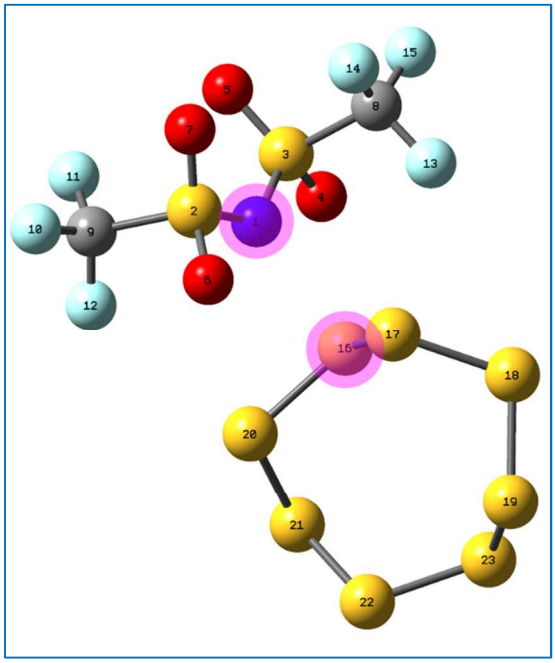

The molecular environment affects the oxidation properties of solvent and additives.